GAGTCCACCTTGCG-3′, rat 18s (F) 5′-GCAATTATTCCCCAT-GAACGA-3′, rat 18s (R) 5′-CAAAGGGCAGGGACTTAATCAAC-3′, probe: 5′-AATTCCCAGTAAGTGCGGGTCATAAGCTTG-3′, mouse 18s (F) 5′-CGCGCAAATTACCCACTCCCGA-3′, mouse 18s (R) 5′-CGGCTACCACATCCAAGGA-3′, probe; 5′-CCAATTACAGGGCCTC-GAAA-3′.

Statistical analysis. Data are expressed as means ± SE. Comparison between or among groups was assessed by Student's *t*-test or ANOVA with Fisher's protected least significant difference test. $P < 0.05$ was considered statistically significant. The χ^2-test was used for analysis of genotype and sex ratio using Microsoft Excel. $P < 0.05$ was considered statistically significant.

RESULTS

Generation of a novel genetically obese rat with a homozygous nonsense mutation in the leptin gene. By using ENU mutagenesis followed by MuT-POWER screening of the KURMA samples (17), we generated a genetically obese *Lep*^{mkyo}/*Lep*^{mkyo} rat with a homozygous nonsense mutation in the leptin gene. *Lep*^{mkyo} mutation was a C-to-T transition at nucleotide 274 in the third exon of leptin gene, resulted to a substitution of glutamine at codon 92 by the stop codon (Q92X), which is upstream of the mutation (R105X) in *Lep*^{ob}/*Lep*^{ob} mice (28) (Fig. 1). Male and female *Lep*^{mkyo}/+ rats were intercrossed to obtain WT, *Lep*^{mkyo}/+, and *Lep*^{mkyo}/*Lep*^{mkyo} animals. There were 27 homozygous WT, 40 *Lep*^{mkyo}/+, and 16 *Lep*^{mkyo}/*Lep*^{mkyo} rats. This ratio did not differ significantly from the expected 1:2:1 Mendelian ratio of genotypes (delivery $n = 8$, mean n of pups per delivery = 10.25; $\chi^2 = 3.17$, $P = 0.999$). The sex ratios also did not differ significantly from the expected ratio (male $n = 42$, female $n = 40$, $\chi^2 = 2.42$, $P = 0.93$).

Plasma leptin concentration and obese phenotypes in Lep^{mkyo}/*Lep*^{mkyo} *rats.* ELISA did not detect plasma leptin in *Lep*^{mkyo}/*Lep*^{mkyo} rats (Fig. 2*A*). Serum leptin concentration in *Lep*^{mkyo}/+ rats (7.81 ± 0.74 ng/ml) was slightly higher than half that of WT rats (12.17 ± 0.72 ng/ml). The body weight in *Lep*^{mkyo}/*Lep*^{mkyo} rats was significantly heavier than WT rats as early as 5 wk of age (Fig. 2*B*). The difference in body weight between WT and *Lep*^{mkyo}/*Lep*^{mkyo} rats steadily widened throughout the study period. The body weight in *Lep*^{mkyo}/+ rats was always slightly heavier than that in WT rats although the difference was not statistically significant. As for the body length, there was no difference between WT and *Lep*^{mkyo}/*Lep*^{mkyo} rats (22.63 ± 0.13 cm in WT rats and 22.69 ± 0.24 cm in *Lep*^{mkyo}/*Lep*^{mkyo} rats, $n = 7$, $P = 0.86$), unlike *Lep*^{ob}/*Lep*^{ob} mice in which the body length is 5–10% shorter than that in lean littermates (3). The gross appearances of WT, *Lep*^{mkyo}/+, and *Lep*^{mkyo}/*Lep*^{mkyo} rats at the age of 19 wk are shown in Fig. 2*C*. The body composition was examined with computer tomography (Fig. 2*D*). In *Lep*^{mkyo}/*Lep*^{mkyo} rats, the subcutaneous fat mass was nearly four times and the intra-abdominal fat mass was nearly twice of those in WT rats. Both subcutaneous fat mass and intra-abdominal fat mass in *Lep*^{mkyo}/+ rats were slightly greater than those in WT rats. Daily food intake in *Lep*^{mkyo}/*Lep*^{mkyo} rats was increased by ~50% compared with WT rats (Fig. 2*E*). The mean body temperature in *Lep*^{mkyo}/*Lep*^{mkyo} rats was significantly lower than that in WT rats (Fig. 2*F*). There was no significant difference between WT and *Lep*^{mkyo}/+ rats in both food intake and body temperature.

Glucose and lipid metabolism in Lep^{mkyo}/*Lep*^{mkyo} *rats.* We performed intraperitoneal glucose tolerance test (Fig. 3, *A* and *B*). Before glucose load, both plasma glucose and insulin concentrations in *Lep*^{mkyo}/*Lep*^{mkyo} rats were already increased when compared with those in WT rats. Plasma glucose concentration in response to the glucose load in *Lep*^{mkyo}/*Lep*^{mkyo} rats was also significantly higher than WT rats. Moreover, the increment of plasma insulin concentration was sustained after glucose load in *Lep*^{mkyo}/*Lep*^{mkyo} rats. These results indicate that the main cause of the impairment of glucose tolerance in *Lep*^{mkyo}/*Lep*^{mkyo} rats was insulin resistance. No significant difference between WT and *Lep*^{mkyo}/+ rats in both plasma glucose and insulin concentrations was observed during glucose tolerance test.

Compared with WT rats, the fasting plasma triglyceride concentration in *Lep*^{mkyo}/*Lep*^{mkyo} rats was markedly elevated (Fig. 3*C*). The NEFA concentration was also increased in *Lep*^{mkyo}/*Lep*^{mkyo} rats although there was no significant difference (Fig. 3*D*). Plasma total cholesterol concentration was significantly increased in *Lep*^{mkyo}/*Lep*^{mkyo} rats (Fig. 3*E*). There was no significant difference between WT and *Lep*^{mkyo}/+ rats in any of these plasma lipid concentrations.

Liver phenotype in Lep^{mkyo}/*Lep*^{mkyo} *rats.* In *Lep*^{mkyo}/*Lep*^{mkyo} rats, the liver was markedly enlarged and lighter in color than that in WT rats. Histological examination of the liver showed large number of lipid droplets of various sizes in *Lep*^{mkyo}/*Lep*^{mkyo} rats (Fig. 3*F*). There was no accumulation of lipid droplets in *Lep*^{mkyo}/+ rats. Consistent with these observations, both liver weight and liver triglyceride content in *Lep*^{mkyo}/*Lep*^{mkyo} rats were markedly increased compared with those in WT rats (Fig. 3, *G* and *H*). There was no significant difference between WT and *Lep*^{mkyo}/+ rats in both liver weight and liver triglyceride content.

Identification of leptin-responsive genes in the liver by microarray analyses. To identify leptin-responsive genes in the liver, we compared gene expressions in the liver between *Lep*^{mkyo}/*Lep*^{mkyo} rats and their WT littermates, as well as leptin-treated and saline-treated *Lep*^{mkyo}/*Lep*^{mkyo} rats, by the microarray method. In the leptin administration experiment, to avoid the effect of chronic

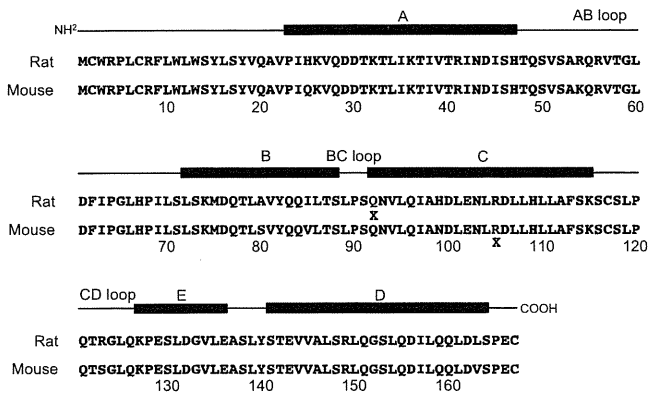

Fig. 1. Mutation (Q92X) in *Lep*^{mkyo}/*Lep*^{mkyo} rats is upstream of the mutation (R105X) in *Lep*^{ob}/*Lep*^{ob} mice. Secondary structure elements (*top*) of leptin precursor and its amino acid sequence in rat (*middle*) and mouse (*bottom*). There is 96% identity of amino acid sequence between mouse and rat. It consists of 4 antiparallel α-helices (A, B, C, and D), connected by 2 long crossover loops (AB and CD) and 1 short loop (BC). Leptin has a small distorted helical segment E in the CD loop. The red Q in the rat sequence indicates the amino acid position of the Q92X mutation. The red R in the mouse sequence indicates the amino acid position of the R105X mutation.

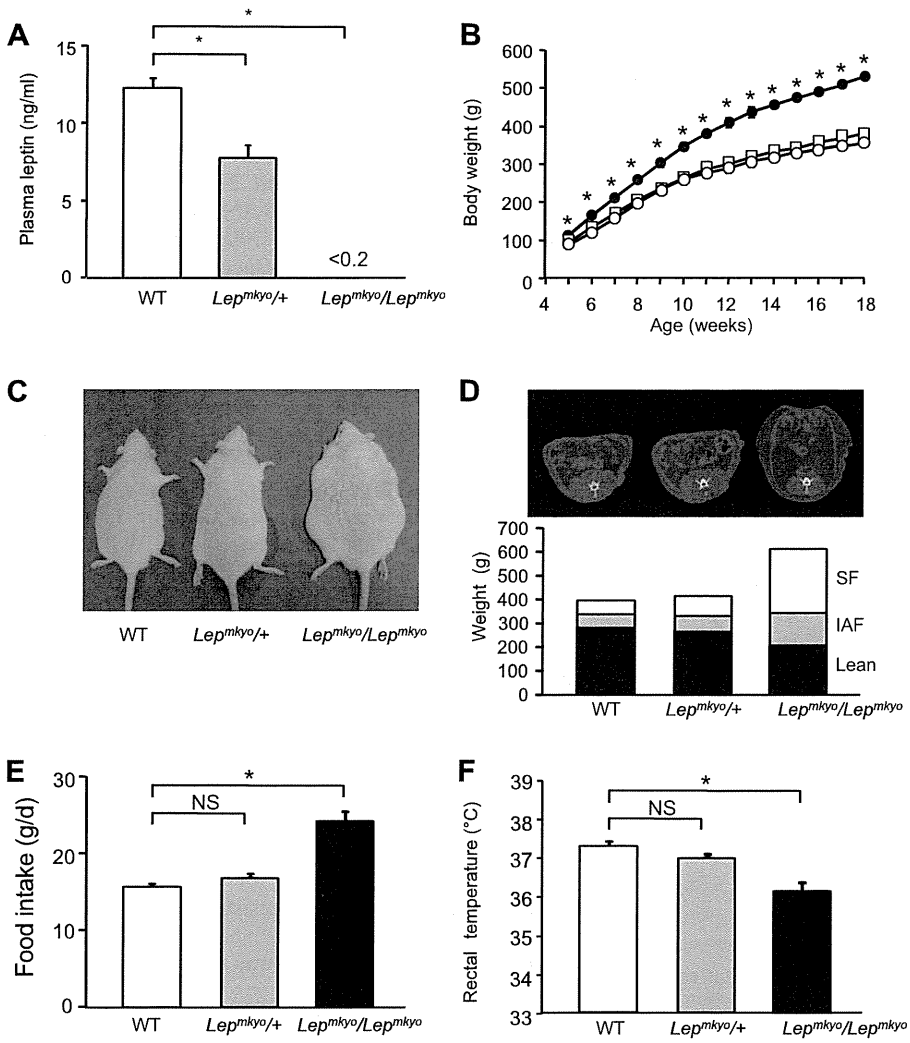

Fig. 2. Obese phenotypes of Lep^{mkyo}/Lep^{mkyo} rats. *A*: plasma leptin concentrations in wild-type (WT, open bar), $Lep^{mkyo}/+$ (gray bar), and Lep^{mkyo}/Lep^{mkyo} (closed bar) rats. Data are means ± SE ($n = 4$ each group). $^*P < 0.01$ (Student's *t*-test). *B*: growth curves in WT (○), $Lep^{mkyo}/+$ (□), and Lep^{mkyo}/Lep^{mkyo} (●) rats. Data are means ± SE ($n = 4$ each group). $^*P < 0.05$ (ANOVA). *C*: gross appearance of WT, $Lep^{mkyo}/+$, and Lep^{mkyo}/Lep^{mkyo} rats. *D*: computer tomography (CT) image at a slice 15 cm distal from nose (*top*) and body composition in WT, $Lep^{mkyo}/+$, and Lep^{mkyo}/Lep^{mkyo} rats (*bottom*). SF, subcutaneous fat mass; IAF, intra-abdominal fat mass; Lean, lean body mass. *E*: daily food intake in WT (open bar), $Lep^{mkyo}/+$ (gray bar), and Lep^{mkyo}/Lep^{mkyo} (closed bar) rats. Daily food intake was measured at the age of 19 wk. Data are means ± SE ($n = 4$ each group). $^*P < 0.05$ (Student's *t*-test). NS, not significant. *F*: rectal temperature in WT (open bar), $Lep^{mkyo}/+$ (gray bar), and Lep^{mkyo}/Lep^{mkyo} (closed bar) rats. Data are means ± SE ($n = 4$ each group). $^*P < 0.05$ (Student's *t*-test).

metabolic changes related to food intake and body weight suppressions by leptin, we administered leptin and started rats fasting at the same time, 6 h before the liver sampling. Moreover, to identify genes that commonly respond to leptin in the liver in rats and mice, we did the same series of experiments with Lep^{ob}/Lep^{ob} mice. We confirmed that there was no significant difference in body weight and plasma glucose, insulin and triglyceride concentrations between leptin-treated and saline-treated Lep^{mkyo}/Lep^{mkyo} rats and also between leptin-treated and saline-treated Lep^{ob}/Lep^{ob} mice (data not shown).

Of 31,042 genes in the rat array chip, we excluded from analysis 18,425 genes with no nomenclature, which could not be found in the mouse array chip, and whose detection calls were not present in any of WT, Lep^{mkyo}/Lep^{mkyo}, and leptin-treated Lep^{mkyo}/Lep^{mkyo} rats. Of the remaining 12,617 genes, 177 genes whose expressions were decreased >1.6-fold in Lep^{mkyo}/Lep^{mkyo} rats relative to WT rats and increased >1.6-fold in leptin-treated Lep^{mkyo}/Lep^{mkyo} rats relative to saline-treated Lep^{mkyo}/Lep^{mkyo} rats were defined as leptin-upregulated genes in rat. However, 138 genes whose expression levels were <100 in either WT or Lep^{mkyo}/Lep^{mkyo} rats were excluded. We defined 237 genes whose expressions were increased >1.6-fold in Lep^{mkyo}/Lep^{mkyo} rats relative to WT rats and decreased >1.6-fold in leptin-treated Lep^{mkyo}/Lep^{mkyo} rats relative to saline-treated Lep^{mkyo}/Lep^{mkyo} rats as leptin-downregulated genes in rat. In this case, 158 genes whose expression levels were <100 in saline-treated Lep^{mkyo}/Lep^{mkyo} rats were excluded from leptin-downregulated genes. Furthermore, among 39 leptin-upregulated genes in rat, six genes whose expression was decreased >1.6-fold in Lep^{ob}/Lep^{ob} mice relative to WT mice and increased >1.0-fold in leptin-treated Lep^{ob}/Lep^{ob} mice relative to saline-treated Lep^{ob}/Lep^{ob} mice were defined as leptin-upregulated genes common in rat and mouse. Among 79 leptin-downregulated genes in rat, 14 genes whose expression were increased >1.6-fold in Lep^{ob}/Lep^{ob} mice relative to WT mice and decreased >1.0-fold in leptin-treated Lep^{ob}/Lep^{ob} mice relative to saline-treated Lep^{ob}/Lep^{ob} mice were defined as leptin-downregulated genes common in rat and mouse.

Expression patterns of these 20 leptin-regulated genes common in rat and mouse were examined by quantitative RT-PCR using the same RNA samples used for microarray analysis. Among six leptin-upregulated genes, *Lin7a* and *Npr2* showed a similar expression pattern in microarray and quantitative RT-PCR analysis (Table 1, Fig. 4*A*). Among 14 leptin-downregulated genes in rats,

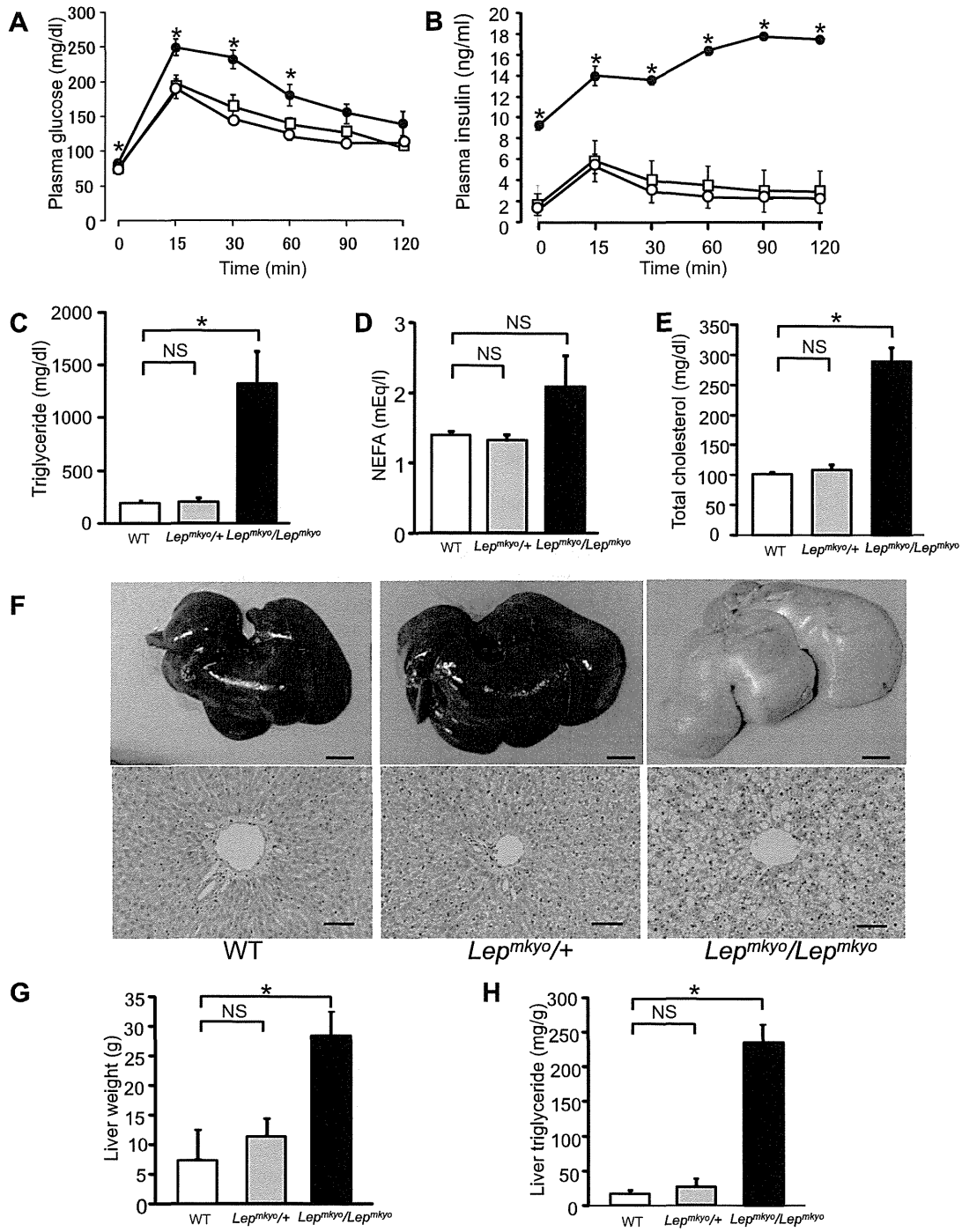

Fig. 3. Glucose, lipid metabolism, and fatty liver in *Lep*^{mkyo}/*Lep*^{mkyo} rats. Plasma glucose (*A*) and insulin concentrations (*B*) at intraperitoneal glucose tolerance test in WT (○), *Lep*^{mkyo}/+ (□), and *Lep*^{mkyo}/*Lep*^{mkyo} (●) rats. Data are means ± SE (n = 4 each group). *$P < 0.05$ (ANOVA). Plasma triglyceride (*C*), nonesterified fatty acid (NEFA, *D*), and total cholesterol (*E*) concentrations in WT (open bar), *Lep*^{mkyo}/+ (gray bar), and *Lep*^{mkyo}/*Lep*^{mkyo} (closed bar) rats. Data are means ± SE (n = 4 each group). *$P < 0.05$ (Student's t-test). *F*: representative macroscopic (*top*: scale bar, 1 cm) and histological (*bottom*: scale bar, 100 μm) sections of the liver in WT, *Lep*^{mkyo}/+, and *Lep*^{mkyo}/*Lep*^{mkyo} rats. For histological examination, hematoxylin and eosin staining was used. Liver weight (*G*) and liver triglyceride contents (*H*) in WT (open bar), *Lep*^{mkyo}/+ (gray bar), and *Lep*^{mkyo}/*Lep*^{mkyo} (closed bar) rats. Data are means ± SE (n = 4 each group). *$P < 0.01$ (Student's t-test).

Table 1. *Microarray analysis data of leptin-responsive genes in the liver*

Gene Name	Gene Symbol	UniGene (Rn.)		Fold Increase			
				Rat		Mouse	
		Rat (Rn.)	Mouse (Mm.)	Wild/Lep^{mkyo}/Lep^{mkyo}	Leptin/vehicle	Wild/*ob/ob*	Leptin/vehicle
Leptin-upregulated gene in liver							
Lin-7 homolog A (*C. elegans*)	Lin7a	31766	268025	2.014	2.158	1.729	1.404
Natriuretic peptide receptor 2	Npr2	32984	103477	2.567	2.25	4.627	1.064
Leptin-downregulated gene in liver							
Chemokine (C-C motif) ligand 2	Ccl2	4772	290320	0.202	0.54	0.17	0.871
Cell division cycle associated 3	Cdca3	129078	285723	0.23	0.207	0.432	0.382
FK506 binding protein 5	Fkbp5	144288	276405	0.219	0.536	0.401	0.774
G protein-coupled receptor 64	Gpr64	57243	213016	0.105	0.574	0.129	0.853
Inhibin beta-B	Inhbb	35074	3092	0.016	0.603	0.33	0.871
Myelocytomatosis oncogene	Myc	12072	2444	0.299	0.473	0.398	0.595
Periplakin	Ppl	25259	266875	0.23	0.547	0.536	0.768

Ccl2, *Cdca3*, *Fkbp5*, *Inhbb*, *C-Myc*, and *Ppl* showed similar expression patterns between microarray and quantitative RT-PCR analysis (Table 1, Fig. 4*B*). These eight genes are expected to play some role in the effect of leptin on the liver.

All microarray data have been deposited at the National Center for Biotechnology Information in the Gene Expression Omnibus database (GEO, http://www.ncbi.nlm.nih.gov/geo/). The series accession number is GSE42532. The GEO platform accession number is GPL1261 in mouse, GPL1355 in rat. The sample accession numbers are GSM 1044286, 1044287, 1044288, 1044289, 1044290, and 1044291.

DISCUSSION

Using gene-driven ENU mutagenesis, we generated leptin-deficient Lep^{mkyo}/Lep^{mkyo} rat. The mutation of leptin gene in Lep^{mkyo}/Lep^{mkyo} rats is located at nucleotide 274 in the third exon of leptin gene, generating a stop codon at amino acid 92 (Q92X), which is upstream of the mutation (R105X) in Lep^{ob}/Lep^{ob} mice (28). Leptin contains two cysteine residues, Cys96 and Cys146, which form a disulfide bond. This disulfide bond was shown to be required for the leptin action (27). Since both sites of nonsense mutation in Lep^{mkyo}/Lep^{mkyo} rats and Lep^{ob}/Lep^{ob} mice were projected to disrupt this disulfide bond, Lep^{mkyo}/Lep^{mkyo} rats were considered to have no functional leptin, as well as Lep^{ob}/Lep^{ob} mice.

The mean mutation frequency with ENU mutagenesis of our protocol was one mutation per 3.7 million base pairs (17). Although the chance for the occurrence of an unexpected mutation with a phenotypic effect is relatively small, this possibility also should be taken account for the experimental design and interpretation of the results. To eliminate mutations that might have been generated by ENU in chromosomal regions other than the *Lep* locus, we performed backcross more than six generations against F344/NSlc inbred background, and we always compared phenotypes between littermates to minimize the effect of possible unexpected mutation.

Lep^{mkyo}/Lep^{mkyo} rats showed morbid obesity with hyperphagia and low body temperature, hyperglycemia with hyperinsulinemia, dyslipidemia, and severely fatty liver. Low body temperature suggests decreased sympathetic nervous activity and basal metabolism in Lep^{mkyo}/Lep^{mkyo} rats. The glucose tolerance test demonstrated marked glucose intolerance with sustained hyperinsulinemia in Lep^{mkyo}/Lep^{mkyo} rats, suggesting insulin resistance. All these phenotypes are consistent with the lack of functional leptin and are identical to those in Lep^{ob}/Lep^{ob} mice (4). There are some existing rat models, such as $Lepr^{fa}/Lepr^{fa}$ Zucker rats and $Lepr^{f}/Lepr^{f}$ Koletzky rats, whose lack of leptin signals is due to mutations in the leptin receptor (22, 23). Although the phenotypes of these rats are also identical to Lep^{mkyo}/Lep^{mkyo} rats, they are not useful in studying the effect of leptin treatment. In this study, we used Lep^{mkyo}/Lep^{mkyo} rat as a leptin-treatable rat model and showed its usefulness.

Generation of leptin knockout rats by pronuclear microinjections of zinc finger nucleases had been reported recently (26). In addition to the metabolic phenotype, those leptin knockout rats with Sprague-Dawley background showed significant increase in bone mineral density and bone volume of the femur compared with WT littermates like *ob/ob* mice (26). However, we could not detect any significant difference in bone mineral density and gross observation of trabecular in the femur by computer tomography between Lep^{mkyo}/Lep^{mkyo} rats and their WT littermates (data not shown). Our result is consistent with the previous report on leptin receptor mutated *fa/fa* rats with Zucker background (24). These results indicate the strain difference in the regulation of bone mineral density. Furthermore, there is a previous report that bone mass in patients with congenital leptin deficiency have normal or low bone mineral density (18), which indicates the species difference. It was also reported that T-cell count was decreased in those leptin knockout rats. In all previous reports of leptin or leptin receptor deficiency in humans (9), mice (16), and rats (25), T-cell count was also decreased. As for the phenotype of T-cell, there is no difference between strains or species, although we did not count the T cells in Lep^{mkyo}/Lep^{mkyo} rats.

Besides the antiobesity effect, leptin has a wide range of metabolic effects including an insulin-sensitizing action. However, the molecular mechanism underlying metabolic effects of leptin is not well understood. We and others have demonstrated that leptin effectively improves insulin sensitivity accompanied by a dramatic reduction of fat content in the liver and skeletal muscle in patients with lipodystrophy in which severely fatty liver and excess fat accumulation in the skeletal muscle frequently develop (5, 6, 8, 15). In this study, to investigate the molecular mechanism by which leptin reduces fat content in the liver, we

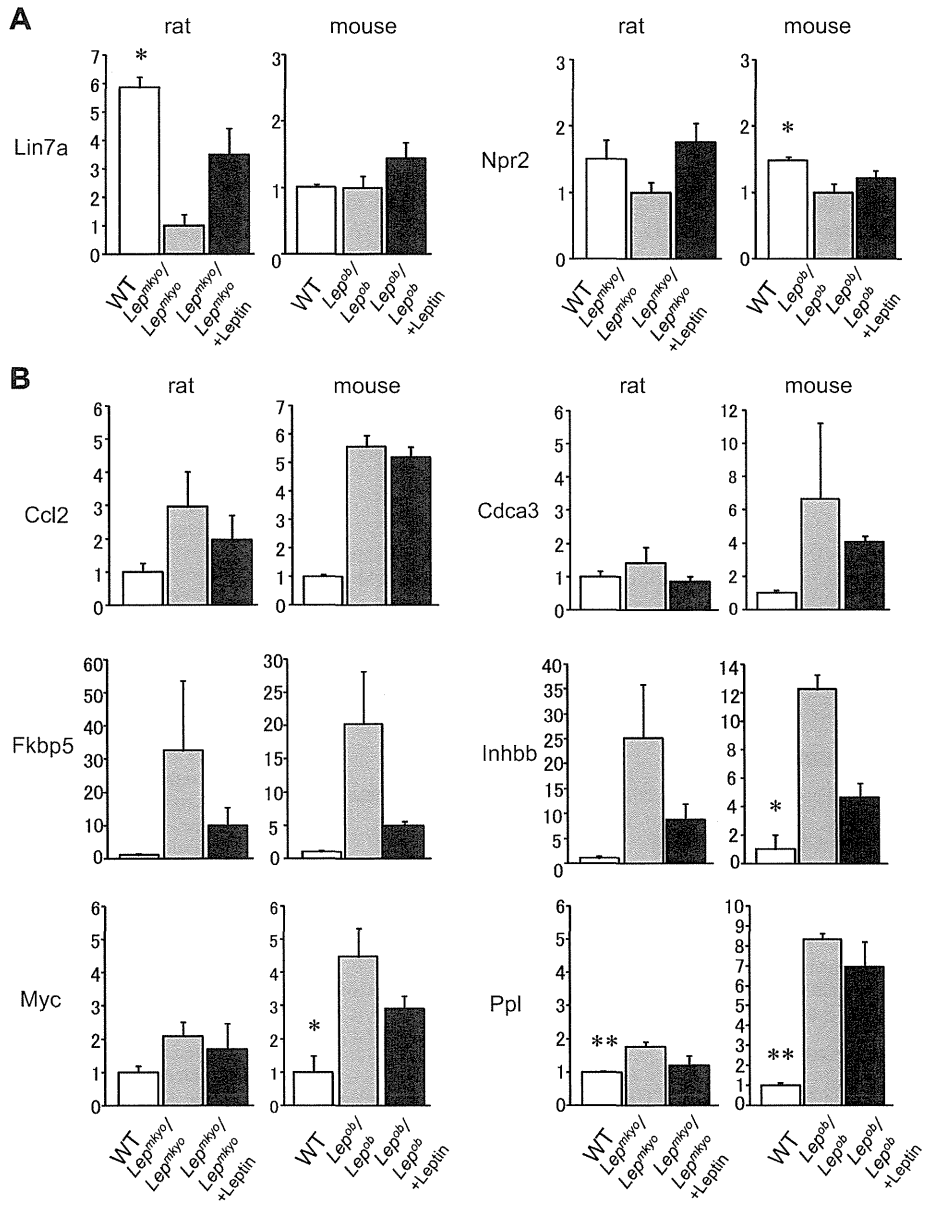

Fig. 4. Reproducibility with quantitative RT-PCR in mRNA expression. The leptin-upregulated genes common in rats and mice (*A*) and leptin-downregulated genes common in rats and mice (*B*) were checked for reproducibility with quantitative RT-PCR. The fold change was displayed as relative to normalized to leptin-deficient animals in *A* and as relative to WT animals in *B*. $^{*}P < 0.05$, $^{**}P < 0.01$ (Student's *t*-test). *Lin7a*, lin-7 homolog A (*C. elegans*), *Npr2*, natriuretic peptide receptor 2; *Ccl2*, chemokine (C-C motif) ligand 2; *Cdca3*, cell division cycle associated 3; *Fkbp5*, FK506 binding protein 5; *Gpr64*, G protein-coupled receptor 64; *Inhbb*, inhibin beta-B; *Myc*, myelocytomatosis oncogene; *Ppl*, periplakin.

used two different species models with leptin deficiency, *Lep*^{mkyo}/*Lep*^{mkyo} rats and *Lep*^{ob}/*Lep*^{ob} mice.

Some microarray analyses on leptin effects in the liver using *Lep*^{ob}/*Lep*^{ob} mice have been reported (2, 14, 19). In these studies, leptin was administrated daily or continuously and the sampling time point was a few days or more after the beginning of leptin treatment. Under these conditions, the investigators could not separate the secondary effects of chronic metabolic changes, such as body weight reduction and improvement of insulin resistance and dyslipidemia, from the primary effects of leptin. In this study, we sampled livers 6 h after leptin administration under fasting. We confirmed that there was no significant difference in body weight and plasma glucose, insulin and triglyceride concentrations between leptin-treated and saline-treated *Lep*^{mkyo}/*Lep*^{mkyo} rats and also between leptin-treated and saline-treated *Lep*^{ob}/*Lep*^{ob} mice. Of course, 6 h after leptin administration is also the limitation of this study. It might be too early to detect leptin-responsive genes. However, we placed priority on excluding secondary effects. As a result, the profile of leptin-responsive genes in the previous report is quite different from that in the present study. In all these previous reports, expression of metabolism-related genes was detected. On the other hand, in our study, all genes in which we detected change of expression were not known for their relationship with glucose or lipid metabolism in the liver. The genes identified in our study are early responsive ones. Identification of such genes might unveil the mechanism of leptin action that has been unknown so far. The mechanistic study of the genes we have identified here is an issue for the future.

In conclusion, we generated leptin-deficient *Lep*^{mkyo}/*Lep*^{mkyo} rats by gene-driven ENU mutagenesis. Taking advantage of leptin-treatable *Lep*^{mkyo}/*Lep*^{mkyo} rats, we compared gene ex-

pressions in the liver not only between *Lep*^{mkyo}/*Lep*^{mkyo} and WT rats, but also between leptin-treated and saline-treated *Lep*^{mkyo}/*Lep*^{mkyo} rats, to identify leptin-responsive genes in the liver by microarray analysis. Taking *Lep*^{mkyo}/*Lep*^{mkyo} rats together with the *Lep*^{ob}/*Lep*^{ob} mice, we finally identified two leptin-upregulated genes, lin-7 homolog A (*Lin7a*) and natriuretic peptide receptor 2 (*Npr2*), and six leptin-downregulated genes, chemokine (C-C motif) ligand 2 (*Ccl2*), cell division cycle associated 3 (*Cdca3*), FK506 binding protein 5 (*Fkbp5*), inhibin beta B (*Inhbb*), myelocytomatosis oncogene (*C-Myc*), and periplakin (*Ppl*). Although, little is known about the physiological significance of most of these genes in energy metabolism in the liver, the analysis of these genes will bring further understanding of leptin physiology in the future.

ACKNOWLEDGMENTS

We thank Keiko Hayashi for technical assistance. The authors also acknowledge Yoko Koyama for secretarial assistance.

GRANTS

This work was supported by research grants from the Japanese Ministry of Education, Culture, Sports, Science, and Technology, the Japanese Ministry of Health, Labor and Welfare, Uehara Memorial Foundation, Grant-in-aid for Industrial Technology Research Grant Program in 2008 from the New Energy and Industrial Technology Development Organization of Japan (TM:08A02004a), and The European Community's Seventh Framework Programme (FP7/2007-2013) under grant agreement no. HEALTH-F4-2010-241504 (EURATRANS).

DISCLOSURES

No conflicts of interest, financial or otherwise, are declared by the author(s).

AUTHOR CONTRIBUTIONS

Author contributions: M.A.-A., K.E., and K.N. conception and design of research; M.A.-A., K.E., C.E., T.M., A.T., and T.T. performed experiments; M.A.-A. and K.E. analyzed data; M.A.-A., K.E., T.M., T.K., Y.Y., D.A., S.Y.-K., T. Sakai, and K.H. interpreted results of experiments; M.A.-A. prepared figures; M.A.-A. and K.E. drafted manuscript; M.A.-A., K.E., and T. Serikawa edited and revised manuscript; T. Serikawa and K.N. approved final version of manuscript.

REFERENCES

1. **Campfield LA, Smith FJ, Guisez Y, Devos R, Burn P.** Recombinant mouse OB protein: evidence for a peripheral signal linking adiposity and central neural networks. *Science* 269: 546–549, 1995.
2. **Cohen P, Miyazaki M, Socci ND, Hagge-Greenberg A, Liedtke W, Soukas AA, Sharma R, Hudgins LC, Ntambi JM, Friedman JM.** Role for stearoyl-CoA desaturase-1 in leptin-mediated weight loss. *Science* 297: 240–243, 2002.
3. **Cone RD.** The melanocortin-4 receptor. In: *The Melanocortin Receptors*, edited by Cone RD. Totowa, NJ: Humana, 2000, p. 404–445.
4. **Dubuc PU.** The development of obesity, hyperinsulinemia, and hyperglycemia in *ob/ob* mice. *Metabolism* 25: 1567–1574, 1976.
5. **Ebihara K, Kusakabe T, Hirata M, Masuzaki H, Miyanaga F, Kobayashi N, Tanaka T, Chusho H, Miyazawa T, Hayashi T, Hosoda K, Ogawa Y, DePaoli AM, Fukushima M, Nakao K.** Efficacy and safety of leptin-replacement therapy and possible mechanisms of leptin actions in patients with generalized lipodystrophy. *J Clin Endocrinol Metab* 92: 532–541, 2007.
6. **Ebihara K, Ogawa Y, Masuzaki H, Shintani M, Miyanaga F, Aizawa-Abe M, Hayashi T, Hosoda K, Inoue G, Yoshimasa Y, Gavrilova O, Reitman ML, Nakao K.** Transgenic overexpression of leptin rescues insulin resistance and diabetes in a mouse model of lipoatrophic diabetes. *Diabetes* 50: 1440–1448, 2001.
7. **Evans MJ, Kaufman MH.** Establishment in culture of pluripotential cells from mouse embryos. *Nature* 292: 154–156, 1981.
8. **Farooqi IS, Jebb SA, Langmack G, Lawrence E, Cheetham CH, Prentice Hughes IA AM, McCamish MA, O'Rahilly S.** Effects of recombinant leptin therapy in a child with congenital leptin deficiency. *N Engl J Med* 341: 879–884, 1999.
9. **Farooqi IS, Matarese G, Lord GM, Keogh JM, Lawrence E, Agwu C, Sanna V, Jebb SA, Perna F, Fontana S, Lechler RI, DePaoli AM, O'Rahilly S.** Beneficial effects of leptin on obesity, T cell hyporesponsiveness, and neuroendocrine/metabolic dysfunction of human congenital leptin deficiency. *J Clin Invest* 110: 1093–103, 2002.
10. **Hedbacker K, Birsoy K, Wysocki RW, Asilmaz E, Ahima RS, Farooqi IS, Friedman JM.** Antidiabetic effects of *IGFBP2*, a leptin-regulated gene. *Cell Metab* 11: 11–22, 2010.
11. **Hillebrand JJ, Langhans W, Geary N.** Validation of computed tomographic estimates of intra-abdominal and subcutaneous adipose tissue in rats and mice. *Obesity* 18: 848–853, 2010.
12. **Hirabayashi M, Kato M, Aoto T, Ueda M, Hochi S.** Rescue of infertile transgenic rat lines by intracytoplasmic injection of cryopreserved round spermatids. *Mol Reprod Dev* 62: 295–299, 2002.
13. **Kamohara S, Burcelin R, Halaas JL, Friedman JM, Charron MJ.** Acute stimulation of glucose metabolism in mice by leptin treatment. *Nature* 389: 374–377, 1997.
14. **Li X, Wu X, Camacho R, Schwartz GJ, LeRoith D.** Intracerebroventricular leptin infusion improves glucose homeostasis in lean type 2 diabetic MKR mice via hepatic vagal and non-vagal mechanisms. *PLoS One* 6: e17058, 2011.
15. **Liang CP, Tall AR.** Transcriptional profiling reveals global defects in energy metabolism, lipoprotein, and bile acid synthesis and transport with reversal by leptin treatment in *ob/ob* mouse liver. *J Biol Chem* 276: 49066–49076, 2001.
16. **Lord GM, Matarese G, Howard JK, Baker RJ, Bloom SR, Lechler RI.** Leptin modulates the T-cell immune response and reverses starvation-induced immunosuppression. *Nature* 394: 897–901, 1998.
17. **Mashimo T, Yanagihara K, Tokuda S, Voigt B, Takizawa A, Nakajima R, Kato M, Hirabayashi M, Kuramoto T, Serikawa T.** An ENU-induced mutant archive for gene targeting in rats. *Nat Gen* 40: 514–515, 2008.
18. **Ozata M, Ozdemir IC, Licinio J.** Human leptin deficiency caused by a missense mutation: multiple endocrine defects, decreased sympathetic tone, and immune system dysfunction indicate new targets for leptin action, greater central than peripheral resistance to the effects of leptin, and spontaneous correction of leptin-mediated defects. *J Clin Endocrinol Metab* 84: 3686–3695, 1999.
19. **Petersen KF, Oral EA, Dufour S, Befroy D, Ariyan C, Yu C, Cline GW, DePaoli AM, Taylor SI, Gorden P, Shulman GI.** Leptin reverses insulin resistance and hepatic steatosis in patients with severe lipodystrophy. *J Clin Invest* 109: 1345–1350, 2002.
20. **Prieur X, Tung YC, Griffin JL, Farooqi IS, O'Rahilly S, Coll AP.** Leptin regulates peripheral lipid metabolism primarily through central effects on food intake. *Endocrinology* 149: 5432–5439, 2008.
21. **Sharma A, Bartell SM, Baile CA, Chen B, Podolsky RH, McIndoe RA, She JX.** Hepatic gene expression profiling reveals key pathways involved in leptin-mediated weight loss in *ob/ob* mice. *PLoS One* 5: e12147, 2010.
22. **Takaya K, Ogawa Y, Isse N, Okasaki T, Satoh N, Masuzaki H, Mori K, Tamura N, Hosoda K, Nakao K.** Molecular cloning of rat leptin receptor isoform complementary DNAs-identification of a missense mutation in Zucker fatty (*fa/fa*) rats. *Biochem Biophys Res Commun* 225: 75–83, 1996.
23. **Takaya K, Ogawa Y, Hiraoka J, Hosoda K, Yamori Y, Nakao K, Koletsky RJ.** Nonsense mutation of leptin receptor in the obese spontaneously hypertensive Koletsky rat. *Nat Genet* 14: 130–131, 1996.
24. **Tamasi JA, Arey BJ, Bertolini DR, Feyen JH.** Characterization of bone structure in leptin receptor-deficient Zucker (*fa/fa*) rats. *J Bone Miner Res* 18: 1605–1611, 2003.
25. **Tanaka S, Isoda F, Yamakawa T, Ishihara M, Sekihara H.** T lymphopenia in genetically obese rats. *Clin Immunol Immunopathol* 86: 219–225, 1998.
26. **Vaira S, Yang C, McCoy A, Keys K, Xue S, Weinstein EJ, Novack DV, Cui X.** Creation and preliminary characterization of a leptin knockout rat. *Endocrinology* 153: 5622–5628, 2012.
27. **Zhang F, Basinski MB, Beals JM, Briggs SL, Churgay LM, Clawson DK, DiMarchi RD, Furman TC, Hale JE, Hsiung HM, Schoner BE, Smith DP, Zhang XY, Wery JP, Schevitz RW.** Crystal structure of the obese protein leptin-E100. *Nature* 387: 206–209, 1997.
28. **Zhang Y, Proenca R, Maffei M, Barone M, Leopold L, Friedman JM.** Positional cloning of the mouse obese gene and its human homologue. *Nature* 372: 425–432, 1994.

STEM CELLS AND DEVELOPMENT
Volume 22, Number 21, 2013

DOI: 10.1089/scd.2013.0113

In Vitro Characterization and Engraftment of Adipocytes Derived from Human Induced Pluripotent Stem Cells and Embryonic Stem Cells

Michio Noguchi,[1] Kiminori Hosoda,[1] Maiko Nakane,[1] Eisaku Mori,[1] Kazuhiro Nakao,[1] Daisuke Taura,[1] Yuji Yamamoto,[1] Toru Kusakabe,[1] Masakatsu Sone,[1] Hidetoshi Sakurai,[2] Junji Fujikura,[1] Ken Ebihara,[1] and Kazuwa Nakao[1]

Human induced pluripotent stem (iPS) and embryonic stem (ES) cells can differentiate into a variety of cell types. We reported on adipogenic potential of human iPS and ES cells in vitro. In the present study, we investigate the survival and maintenance of adipocytes differentiated in vitro from human iPS and ES cells after transplantation. Following adipogenic induction in vitro, the differentiated cells exhibited functional properties of adipocytes such as lipid storage, lipolysis, and insulin responsiveness. Subsequently, Matrigel containing the differentiated human iPS and ES cells was transplanted into the subcutaneous tissue of nude mice. After 1–4 weeks, the cells with adipocyte-like features were observed in transplanted Matrigel by histological analysis. The human origin of the cells, their lipid accumulation, and gene expression of adipocyte markers in transplanted cells were then confirmed, suggesting the presence of adipocytes in transplanted Matrigel. When the relative areas of these cells were calculated by dividing the adipocyte areas by the total Matrigel areas, we found that they peaked at 2 weeks after transplantation, and that the adipocytes persisted at 4 weeks. The present study demonstrates that human iPS and ES cells can differentiate into adipocytes with functional properties and that adipocytes derived from human iPS and ES cells can survive and maintain the differentiated properties of adipocytes for at least 4 weeks after transplantation. Adipocytes derived from human iPS and ES cells thus have the potential to open new avenues for stem cell-based research into metabolic diseases and future therapeutic applications.

Introduction

Human induced pluripotent stem (iPS) cells exhibit pluripotency in vitro and in vivo like that seen with human embryonic stem (ES) cells [1–3]. Moreover, human iPS cells have been differentiated into a variety of cell types [4–12]. For example, we demonstrated that both human iPS and ES cells have adipogenic potential in vitro [13]. On the other hand, studies involving the transplantation of human iPS cell derivative have been limited to only a few cell types [14–17]. Transplantation studies of derivatives from human PS cells become increasingly important to explore a novel cell therapy for intractable diseases.

Lipodystrophy is a rare syndrome characterized by loss of adipose tissue, which causes insulin resistance, diabetes, dyslipidemia, and ectopic fat accumulation [18,19]. Transplantation of adipose tissue ameliorates the phenotype of lipodystrophy [20]. Further, adipose tissue, adipocytes, and adipose-derived stem cells are therapeutically useful for soft tissue reconstruction after tumor resection [21–24]. Adipocytes derived from human PS cells can be a possible source of cell therapy for lipodystrophy and soft tissue reconstruction. To date, there have been several reports of using scaffolds to construct adipose-like tissue derived from human adult stem cells and embryonic germ cells [25–28]; however, construction of adipose-like tissue derived from human iPS and ES cells has not been fully demonstrated.

In the present study, we initially assessed functional properties of adipocytes such as lipid storage, lipolysis, and insulin responsiveness in vitro in differentiated human iPS and ES cells. We then studied survival and maintenance of adipocytes derived from human iPS and ES cells following their transplantation.

Materials and Methods

Cell culture

Human iPS cells: 253G4 (G4), 201B7 (B7), and W12, were maintained in a Primate ES medium (ReproCELL) supplemented with 4 ng/mL recombinant human basic fibroblast growth factor (Invitrogen) as we previously described [13]. G4 and B7 were kindly provided by Shinya

[1]Department of Medicine and Clinical Science, Kyoto University Graduate School of Medicine, and [2]Center for iPS Cell Research and Application (CiRA), Kyoto University, Kyoto, Japan.

Yamanaka [29]. Human ES cells (H9 and KhES-1) were cultured as described previously [29]. H9 was purchased from Wicell Research Institute, Inc. KhES-1 was kindly provided by Norio Nakatsuji [30]. W12 as well as B7 were generated from human dermal fibroblasts from a 36-year-old Caucasian woman (Cell Applications, Inc.) by introducing four factors, such as Oct3/4, Sox2, Klf4, and c-Myc. Expression of human ES cell markers and pluripotency were examined by immunocytochemistry, in vitro differentiation, and teratoma formation (Supplementary Fig. S1A–K; Supplementary Data are available online at www.liebertpub.com/scd) according to the methods described previously [1]. Standard G-banding chromosome analysis was performed in the Nihon Gene Research Laboratories, Inc. (Supplementary Fig. S1L). Human bone marrow-derived mesenchymal stem cells were purchased from Lonza. Adipogenic differentiation was induced according to the manufacturer's instruction.

Adipogenic differentiation of human iPS and ES cells

Human iPS and ES cells were differentiated into the adipocyte lineage via embryoid body (EB) formation using a modified version of the protocol, which we previously described [13]. Briefly, adipogenic differentiation was initiated by aggregation of iPS and ES cells to form EBs. From day 2–5, retinoic acid (SIGMA-Aldrich) with the concentration of 100 nM was supplemented. From day 8–11, 1 μg/mL insulin (Roche Diagnostics) and 1 μM pioglitazone (SIGMA-Aldrich) were supplemented. After 11 days of EB culture, EBs were transferred to plates coated with type IV collagen (BD Biosciences). Adipogenic differentiation was induced for additional 3–5 days of culture using 10% fetal bovine serum/Dulbecco's Modified Eagle Medium (DMEM) containing 0.5 mM 3-isobutyl-1-methylxanthine (Nacalai Tesque), 0.25 μM dexamethasone (Nacalai Tesque), 1 μg/mL insulin, and 1 μM pioglitazone.

Oil Red O staining

Differentiated human iPS and ES cells were washed with phosphate-buffered saline (PBS) twice, fixed in 3.7% formaldehyde for 1 h, and then stained with a 0.6% (w/v) Oil Red O solution (60% isopropanol and 40% water) for 2 h at room temperature. Cells were then washed with water to remove unbound dye. Optical sections were obtained with BZ-9000 (KEYENCE). Oil Red O-stained areas were calculated as the percentage of the area divided by the total area.

Immunocytochemistry

Differentiated human iPS and ES cells were washed with PBS and fixed for 10 min with 4% paraformaldehyde. Then, the cells were permeabilized by 0.1% Triton X in PBS for 5 min and incubated by Protein Block (DAKO) for 30 min at room temperature. The cells were immunostained with a 1:200 dilution of a primary antibody against peroxisome proliferator-activated receptor γ (PPARγ; Cell Signaling Technology). After washed with PBS, Alexa 546-conjugated anti-rabbit IgG (Molecular Probes) was used as a secondary antibody with the concentration of 10 μg/mL. Then, after being washed with PBS, BODIPY 493/503 (Molecular Probes) was added for 15 min for lipid staining. The cells were mounted in the medium with 4′,6-diamidino-2-phenylindole after washed with PBS twice (Vector Labs). Then, human iPS cells were stained with primary antibodies against Nanog (1:20; R&D Systems), TRA-1-60 (1:100; Millipore), SSEA-4 (1:100; Santa Cruz Biotechnology, Inc.), β3-tubulin (1:100; Millipore), α-smooth muscle actin (pre-diluted; DAKO), and α-fetoprotein (1:100; Millipore) according to the protocol described previously [20]. Alexa Fluor 488-conjugated anti-mouse IgG, Alexa Fluor 546-conjugated anti-goat IgG, and Alexa Fluor 546-conjugated anti-mouse IgG antibodies (Molecular Probes) were used as secondary antibodies with a concentration of 10 μg/mL. An alkaline phosphatase activity was detected using a BCIP/NBT substrate system (DAKO). 3T3-L1 cells and human mesenchymal stem cells were stained with a primary antibody against vimentin (1:100; DAKO). Alexa Fluor 546-conjugated anti-mouse IgG was used as a secondary antibody. Optical sections were obtained with BZ-9000.

Lipolysis assays

Before lipolysis assays, differentiated human iPS and ES cells were incubated in the serum-free DMEM with 0.5% fatty acid-free bovine serum albumin for 4 h. For lipolysis assays, differentiated cells were stimulated with 10 μM forskolin for 6 h. The medium was then collected and established procedures were used to quantify the glycerol as

FIG. 1. Adipogenic differentiation of human iPS and ES cells in vitro. **(A–E)** Oil Red O staining of differentiated human iPS cells **(A:** G4, **B:** B7, **C:** W12**)**, differentiated human ES cells **(D:** H9**)**, and undifferentiated human iPS cells **(E:** W12**)**. Scale bar = 25 μm. **(F)** Gene expression of adipocyte markers in differentiated human iPS and ES cells. Lane 1: undifferentiated iPS cells (B7), lane 2: differentiated G4, lane 3: differentiated B7, lane 4: differentiated H9, lane 5: adipocytes derived from human bone marrow-derived mesenchymal stem cells. **(G–O)** Subcellular localization of PPARγ in differentiated human iPS cells (W12), differentiated human ES cells (H9), and undifferentiated human iPS cells (W12). Lipid staining by BODIPY 493/503 and immunostaining with PPARγ in differentiated iPS cells **(G)**, differentiated ES cells **(J)**, and undifferentiated iPS cells **(M)**. Nuclear staining with 4′,6-diamidino-2-phenylindole in differentiated iPS cells **(H)**, differentiated ES cells **(K)**, and undifferentiated iPS cells **(N)**. Merge sections in differentiated iPS cells **(I)**, differentiated ES cells **(L)**, and undifferentiated iPS cells **(O)**. Scale bar = 20 μm. **(P)** Forskolin-stimulated lipolysis in undifferentiated or differentiated human iPS (W12) and ES (H9) cells. Glycerol release in the culture medium was measured. Data are expressed as mean ± standard error from duplicate experiments ($n = 3$–5). $^*p < 0.05$; $^{**}p < 0.01$ compared with vehicle-treated groups. **(Q)** Insulin-induced AKT phosphorylation in undifferentiated or differentiated human iPS cells (W12) and ES cells (H9). Cells were stimulated with 100 nM or 1 μM insulin for 5 min. FK, forskolin; hiPSCs, undifferentiated human iPS cells; hESCs, undifferentiated human ES cells; dhiPSCs, differentiated human iPS cells; dhESCs, differentiated human ES cells; iPS cells, induced pluripotent stem cells; ES cells, embryonic stem cells; PPARγ, peroxisome proliferator-activated receptor γ.

instructed by the manufacturer (SIGMA-Aldrich). The protein content was determined using Protein Assay (BIORAD).

Western blot analysis

Preparation of total cell lysates and western blot analysis were performed as we previously described [31]. Briefly, cells were harvested in the lysis buffer. For western blot analysis, proteins were subjected to sodium dodecyl sulfate–polyacrylamide gel electrophoresis and transferred to polyvinylidene fluoride membranes. The membranes were immunoblotted with the primary antibodies against AKT and phospho AKT (Ser 473) (Cell Signaling Technology). Membranes were reacted with the secondary antibody (GE Healthcare) and developed with ECL plus (GE Healthcare) as instructed by the manufacturer. The signal on the blot was detected with ImageQuant LAS 4000 System (GE Healthcare).

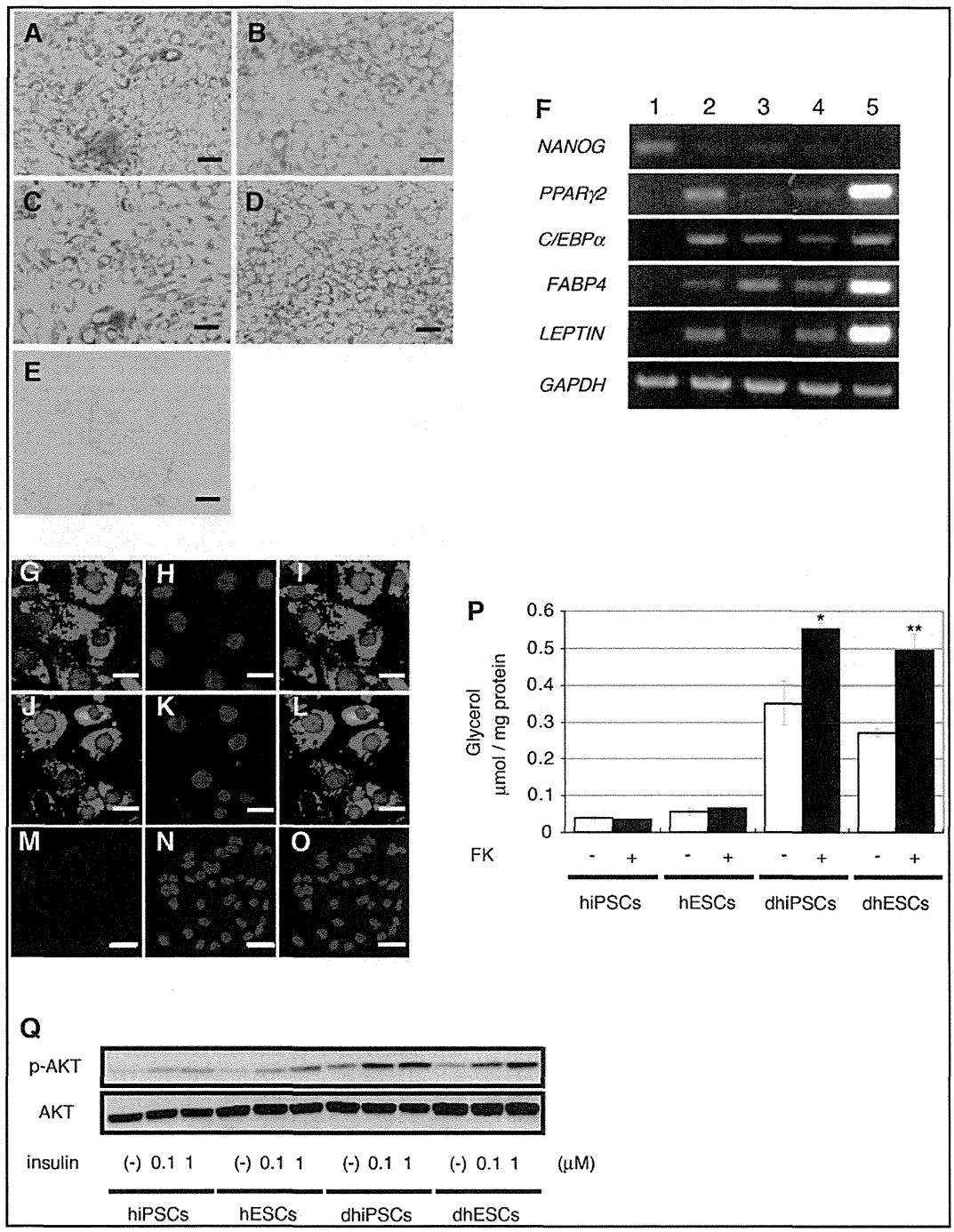

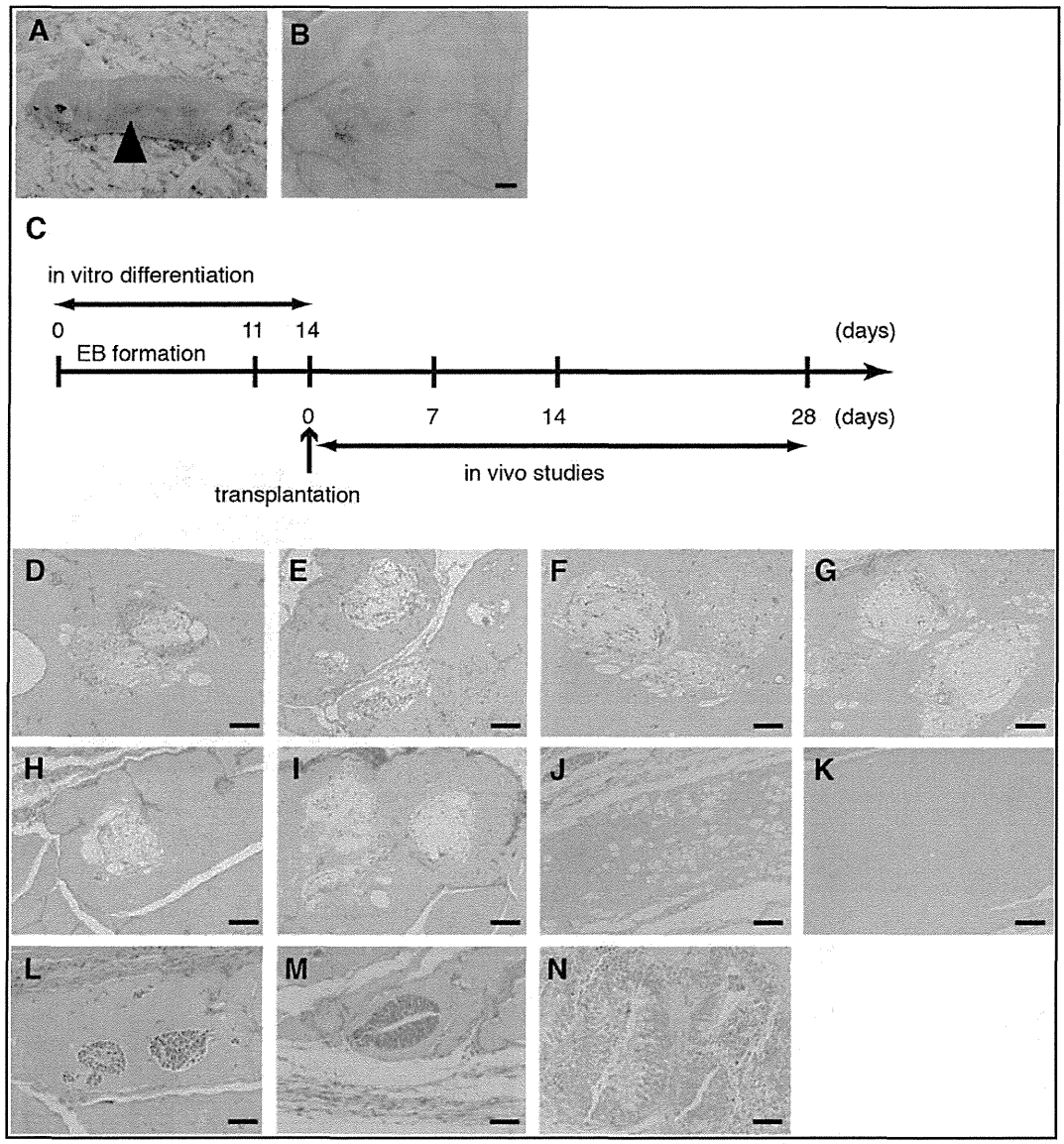

FIG. 2. Transplantation of adipocytes derived from human iPS cells and ES cells. **(A)** Appearance of a BALB/cA nude mouse into which Matrigel containing differentiated human iPS cells was transplanted. The *arrowhead* indicates the transplantation site. **(B)** Appearance of the mouse subcutaneous tissue collected at 2 weeks after transplantation of Matrigel containing differentiated human iPS cells. Scale bar = 2 mm. **(C)** Timeline of transplantation study. After 14 days of in vitro differentiation, differentiated human iPS and ES cells were transplanted. Implanted Matrigel containing differentiated human iPS and ES cells was collected at the indicated time points. **(D–I)** Transplanted cells were stained with hematoxylin and eosin. Morphological features of implanted Matrigel containing differentiated G4 **(D, F, H)** and H9 **(E, G, I)** after 1–4 weeks. **D, E:** 1 week, **F, G:** 2 weeks, **H, I:** 4 weeks. Scale bars = 100 μm. **(J, K)** Morphological features of implanted Matrigel containing adipocytes derived from human mesenchymal stem cells **(J)** and implanted cell-free Matrigel **(K)** after 4 weeks. Scale bars = 100 μm. **(L–N)** Morphological features of implanted Matrigel containing undifferentiated G4 after 1–4 weeks. **L:** 1 week, **M:** 2 weeks, **N:** 4 weeks. Scale bars = 50 μm.

Flow cytometric analysis

At 3 days after attachment of EBs and supplementation of adipogenic cocktails, cells were harvested. Single-cell suspensions were labeled for 30 min on ice with the mouse fluorescence-conjugated antibodies against PE-CD73 and PE-CD105 (eBioscience). The cells were analyzed by FACS-Aria II (BD Biosciences).

Transplantation of derivatives from human iPS cells and ES cells

This study was performed after approval of the Kyoto University Graduate School and Faculty of Medicine, Ethics Committee (No. 824 and ES6). All animal experiments were performed in strict accordance with the guidelines for animal experiments of Kyoto University. Matrigel (BD Biosciences) was

mixed with a suspension of differentiated or undifferentiated human iPS and ES cells harvested from a confluent 100-mm dish. Matrigel incorporating 2×10^7 differentiated or 1×10^7 undifferentiated PS cells was then carefully implanted into the subcutaneous tissue on the backs of 8-week-old male BALB/cA nude mice (CLEA Japan) using a syringe with a 21-gauge needle. Samples of skin tissue, including the implanted Matrigel were harvested for further studies at 1 day, 1 week, 2 weeks, and 4 weeks after transplantation. Matrigel incorporating adipocytes derived from 2×10^6 human bone marrow-derived mesenchymal stem cells was also implanted into the subcutaneous tissue on the backs of the BALB/cA nude mice as a positive control study.

Immunohistochemistry

Human adipose tissue biopsy was performed after approval of the Kyoto University Graduate School and Faculty of Medicine, Ethics Committee (No. 553). Each tissue specimen was fixed in 10% neutralized formalin solution, embedded in paraffin, sectioned at the central portion of implanted Matrigel, and followed by staining with hematoxylin and eosin (HE) or immunohistochemical studies. The paraffin sections were immunostained using the Polymer Immunocomplex System (DAKO) with a 1:50 dilution of a primary antibody against human vimentin (DAKO). Phosphohistone H3 was stained with a 1:100 dilution of the primary antibody (Cell Signaling Technology). Cryosections from the samples were fixed with a 10% neutralized formalin solution before embedding in optimal cutting temperature compound. Lipid accumulation in transplanted cells was assessed by Oil Red O staining. Morphometric analyses were performed using BZ-9000. The relative adipocyte area was expressed as the ratio of the adipocyte area to the total Matrigel area in each section.

Reverse transcription polymerase chain reaction

Total RNA was extracted using the TRIzol reagent (Invitrogen). For reverse transcription polymerase chain reaction (RT-PCR) assay, cDNA was synthesized by iScript (BIORAD). Semiquantitative PCR was carried out using GeneAmp PCR System 9700 as instructed by the manufacturer (Applied Biosystems). TaqMan PCR was performed using Step One Plus Real-Time PCR System as instructed by the manufacturer (Applied Biosystems). Relative levels of mRNA were normalized to the mRNA level of GAPDH. The primers and probes used were listed in Supplementary Fig. S2.

Statistical analysis

The data are presented as mean ± standard error. The Student's *t*-test was used as the statistical analysis. The level of significant difference was the p-value < 0.05.

Results

Adipogenic differentiation of human iPS and ES cells in vitro

Human iPS (G4, B7, and W12) and ES (H9) cells were differentiated into the adipocyte lineage in vitro. Differentiated iPS and ES cells exhibited prominent lipid accumulation by Oil Red O staining, while lipid accumulation was rarely observed in undifferentiated cells (Fig. 1A–E). After differentiation in vitro, gene expression of a set of adipocyte markers, such as PPARγ2, CCAAT/enhancer-binding protein (C/EBP) α, fatty acid-binding protein-4 (FABP4), and leptin, was detected by RT-PCR analysis. Gene expression of Nanog in differentiated cells was markedly lower than in undifferentiated cells (Fig. 1F). Immunohistochemical analysis showed that the PPARγ protein was present within the nuclei of a portion of the differentiated iPS and ES cells containing lipid droplets, while the PPARγ protein was not detected in undifferentiated cells (Fig. 1G–O). Further, these differentiated cells were examined whether they have lipolytic responses and insulin responsiveness. In differentiated cells from both iPS and ES cells, 10 μM forskolin significantly enhanced glycerol release into the culture medium (~1.6-fold and ~1.8-fold increase, respectively), as compared to vehicle-treated groups. In undifferentiated iPS and ES cells, 10 μM forskolin did not significantly increase glycerol release (Fig. 1P). In addition, 100 nM or 1 μM insulin remarkably increased AKT phosphorylation in differentiated iPS and ES cells as compared to vehicle-treated groups. AKT phosphorylation was also slightly enhanced in undifferentiated iPS and ES cells (Fig. 1Q). These findings suggest the presence of adipocytes with functional properties in differentiated iPS and ES cells.

Transplantation of adipocytes derived from human iPS and ES cells

After 14 days of in vitro differentiation, Matrigel containing differentiated human iPS (G4) or ES (H9) cells was transplanted into the subcutaneous tissue on the backs of 8-week-old BALBc/A nude mice (Fig. 2A). Matrigel containing undifferentiated iPS cells or cell-free Matrigel was transplanted as a negative control, while Matrigel containing adipocytes derived from human bone marrow-derived mesenchymal stem cells was transplanted as a positive control. At 1 day, 1 week, 2 weeks, and 4 weeks after transplantation, samples of skin tissue containing the Matrigel were harvested. Grossly, small blood vessels could be seen distributed in Matrigel (Fig. 2B). Timeline of the transplantation study was demonstrated (Fig. 2C). Preparation of histological sections and HE staining of specimens collected at 1 week after transplantation revealed that the differentiated iPS or ES cells possess adipocyte-like features, including thin rims of cytoplasm surrounding the vacuole and flattened nucleus (Fig. 2D, E). Similar histological findings were observed at 2 and 4 weeks after transplantation of differentiated iPS and ES cells (Fig. 2F–I). These cells were also noted at 4 weeks after transplantation of adipocytes derived from human mesenchymal stem cells (Fig. 2J), but no adipocytes described above were observed in cell-free Matrigel at 4 weeks after transplantation (Fig. 2K). By contrast, adipocytes derived from human iPS and ES cells were rarely seen at 1 day after transplantation (data not shown), which may indicate the loss of lipid droplets caused by the transplantation procedure and insufficient vascularization in the Matrigel at that time. Histological findings also showed that Matrigel with undifferentiated human iPS cells mainly contained immature neuroectodermal cells such as neural tube cells at 1, 2, and 4 weeks after transplantation (Fig. 2L–N). No adipocytes described above were detected throughout the transplantation period.

Characterization of transplanted cells derived from human iPS and ES cells

We next calculated the relative areas of the adipocytes by dividing the adipocyte area by the total Matrigel area in sections of skin tissue collected at 1 day, 1 week, 2 weeks, and 4 weeks after transplantation of differentiated human iPS and ES cells. The areas were 0.63%±0.10% (G4) and 0.42%±0.17% (H9) on day 1 after transplantation. At 1 week after transplantation, the relative areas were 2.27%±1.19% (G4) and 9.39%±1.36% (H9), and by 2 weeks after transplantation, they had increased to 5.26%±0.46% (G4) and 12.9%±5.32% (H9). However, the areas had declined to 2.17%±1.28% (G4) and 6.97%±1.66% (H9) at 4 weeks after transplantation (Fig. 3A). Thus, the adipocytes were clearly present at 1–4 weeks after transplantation of differentiated iPS or ES cells, and relative adipocyte areas were maximal at 2 weeks after transplantation.

To assess the proliferative capacity of the transplanted cells, the cells were immunostained with an antibody against phosphohistone H3 at 2 weeks after transplantation. Adipocytes derived from human iPS and ES cells exhibited little or no proliferative capacity (Fig. 3B, C), whereas the immature neuroectodermal cells exhibited a high-proliferative capacity in transplantation of undifferentiated human iPS cells (Fig. 3D).

The origin of the adipocytes in the Matrigel was studied by immunostaining with an antibody against human vimentin. According to the manufacturer's guide and an earlier report [32], the antibody used does not cross react with mouse vimentin. We also evaluated the cross reactivity of the antibody with mouse vimentin. Vimentin was stained with the antibody in human mesenchymal stem cells, while it was not stained in mouse 3T3-L1 cells (Supplementary Fig. S3A–D). Moreover, human subcutaneous adipose tissue was stained with the antibody (Supplementary Fig. S3E), but mouse subcutaneous adipose tissue was not (Supplementary Fig. S3F).

When we then assessed the human vimentin immunoreactivity of the cells within the Matrigel, we found that adipocytes derived from both iPS and ES cells were labeled by the anti-vimentin antibody at 2 and 4 weeks after transplantation (Fig. 4A–H). Further, lipid accumulation in the cells was demonstrated by staining frozen sections with Oil Red O at 2 and 4 weeks after transplantation (Fig. 4I–L). Similar histological findings were observed at 2 weeks after transplantation of adipocytes derived from human bone marrow-derived mesenchymal stem cells (Fig. 4M–O).

Gene expression of a set of adipocyte markers in transplanted differentiated iPS and ES cells was then investigated by PCR analyses. Gene expression of PPARγ2, C/EBPα, aP2, and leptin was detected at 2 and 4 weeks after transplantation (Fig. 5A, B). Quantitative real-time PCR analyses carried out with the samples after transplantation revealed that leptin and PPARγ2 were expressed at 1, 2, and 4 weeks after transplantation. In both iPS and ES cells, mRNA levels of leptin at 1 and 2 weeks after transplantation were higher than those at 4 weeks after transplantation (Fig. 5C). Meanwhile, mRNA levels of PPARγ2 at 4 weeks after transplantation were maintained in both cell lines as compared with those at 2 weeks (Fig. 5D).

Transplantation of other human pluripotent stem cell lines

When we similarly transplanted Matrigel containing other differentiated human iPS cell line (B7 and W12) and another human ES cell line (KhES-1), adipocytes described above were observed at 2 weeks after transplantation, suggesting that adipocytes derived from other PS cells can survive after transplantation (Fig. 6A–C). At that time, the relative areas of adipocytes derived from B7, W12, and KhES-1 were 1.11%±0.57%,

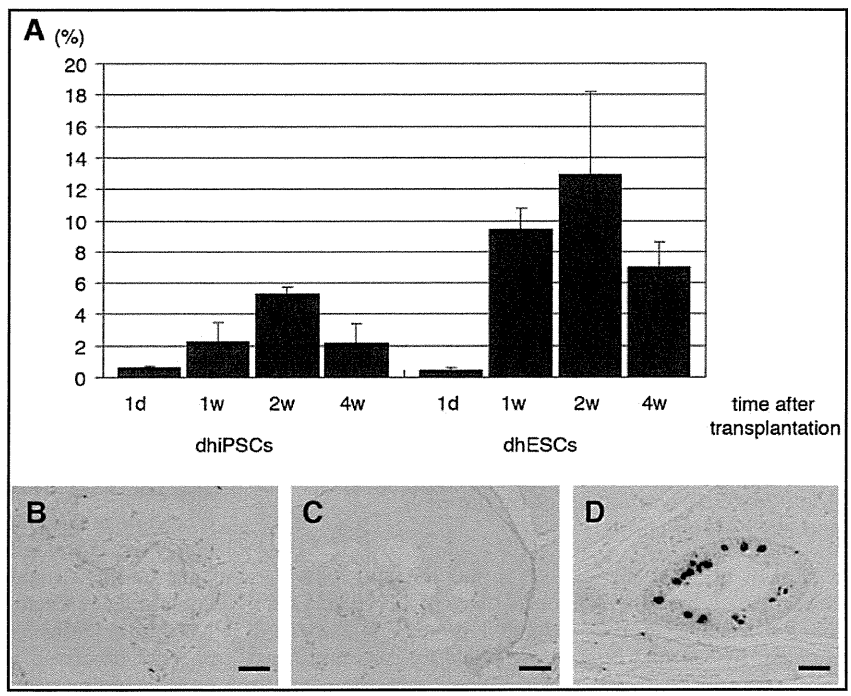

FIG. 3. Quantification of adipocyte areas and proliferative capacity of transplanted cells. **(A)** Relative adipocyte areas at 1 day, 1 week, 2 weeks, and 4 weeks after transplantation of differentiated G4 (dhiPSCs) and differentiated H9 (dhESCs) were shown. Data are expressed as mean±standard error. At least, six sections from three samples were analyzed for each group. 1d: 1 day, 1w: 1 week, 2w: 2 weeks, 4w: 4 weeks. **(B–D)** Proliferative capacity of transplanted cells after 2 weeks. Immunostaining with an antibody against phosphohistone H3 of transplanted cells. Implanted Matrigel containing differentiated G4 **(B)**, differentiated H9 **(C)**, and undifferentiated G4 **(D)**. Scale bars=50 μm.

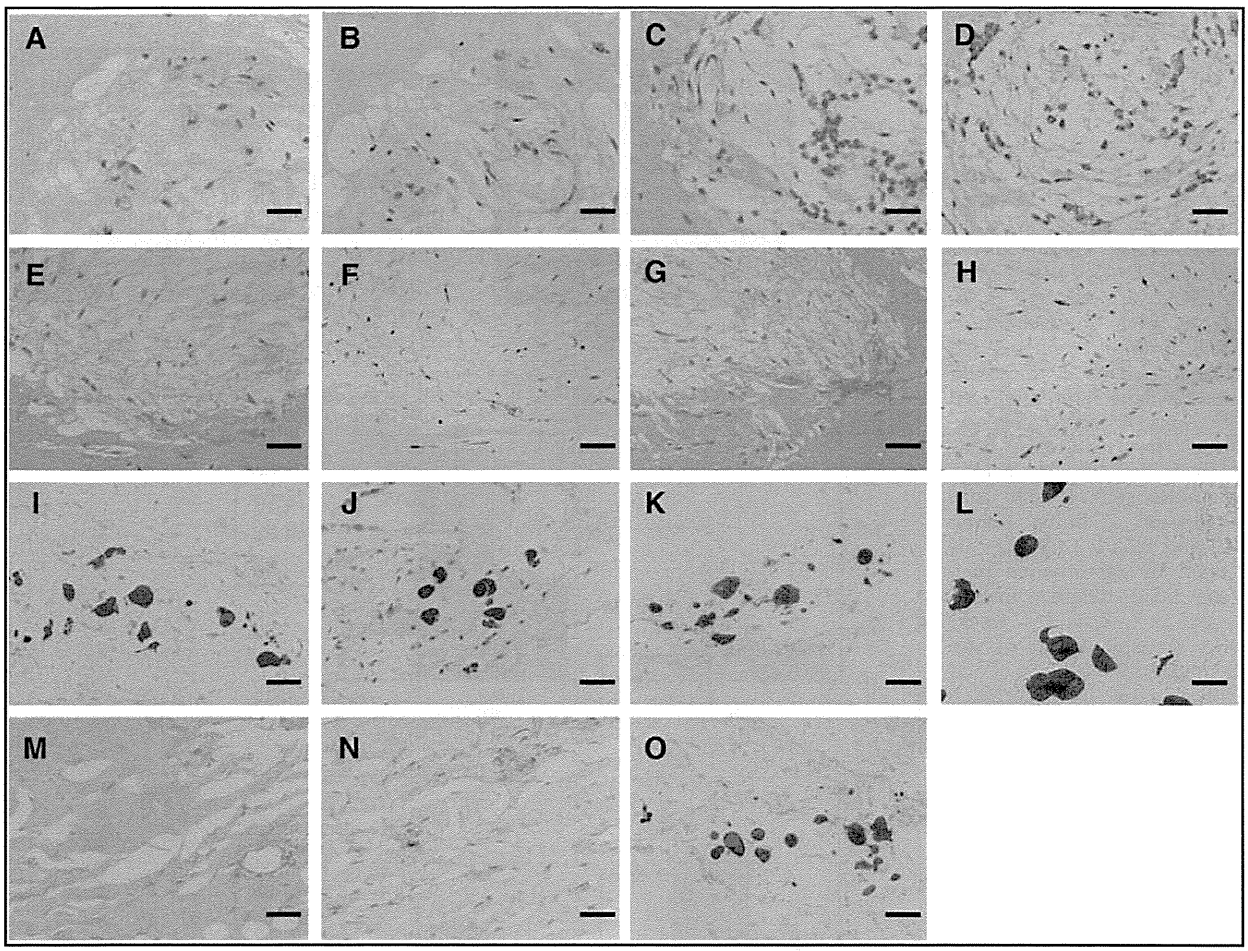

FIG. 4. Human origin and lipid accumulation in transplanted cells. **(A–H)** HE staining **(A, C, E, G)** and immunostaining with an antibody against human vimentin **(B, D, F, H)** of serial sections of transplanted cells after 2 weeks **(A, B:** differentiated G4; **C, D:** differentiated H9**)** and 4 weeks **(E, F:** differentiated G4; **G, H:** differentiated H9**)**. Scale bars = 20 μm. **(I–L)** Oil Red O staining of the frozen sections of transplanted cells after 2 weeks **(I**: differentiated G4, **J:** differentiated H9**)** and 4 weeks **(K**: differentiated G4, **L:** differentiated H9**)**. Scale bars = 50 μm. **(M, N)** HE staining **(M)** and immunostaining with an antibody against human vimentin **(N)** of serial sections of transplanted adipocytes derived from human bone marrow-derived mesenchymal stem cells after 2 weeks. Scale bars = 20 μm. **(O)** Oil Red O staining of the frozen sections of transplanted adipocytes derived from human bone marrow-derived mesenchymal stem cells after 2 weeks. Scale bar = 50 μm. HE, hematoxylin and eosin.

1.45% ± 0.48%, and 2.41% ± 1.42%, respectively (Fig. 6D), much less than were seen with G4 and H9. To examine the adipogenic differentiation rate of in vitro differentiated iPS and ES cells before transplantation, we quantified Oil Red O-stained areas of the differentiated iPS and ES cells. The areas of differentiated G4 and H9 were 23.89% ± 1.28% and 26.51% ± 1.29%, respectively. Moreover, those of differentiated B7, W12, and KhES-1 were 20.92% ± 2.77%, 22.92% ± 0.56%, and 21.25% ± 2.17%, respectively (Supplementary Fig. S4), smaller than those of differentiated G4 and H9.

Discussion

The present study demonstrates that human iPS and ES cells can differentiate into adipocytes with functional properties in vitro and that adipocytes derived from human iPS and ES cells can survive and maintain the differentiated properties in vivo for at least 4 weeks after transplantation.

We and others have reported that human iPS [13,33] and ES [34–40] cells have adipogenic potential in vitro. However, the functional properties of adipocytes derived from human iPS cells have not yet been fully characterized. Lipid storage and lipolysis are considered as major functions of mature adipocytes. Adipocytes store triacylglycerol when energy is in excess, and hydrolyze triacylglycerol to release fatty acids for utilization in other cells in response to energy demand. Triacylglycerol synthesis occurs in various tissues, while lipolysis predominantly occurs in adipose tissue [41]. The present study shows that PPARγ is localized in the nuclei of differentiated human iPS cells containing lipid droplets, and that these cells exhibit forskolin-stimulated lipolytic responses and insulin-induced AKT phosphorylation, suggesting that adipocytes with functional properties, such as lipid storage, lipolysis, and insulin responsiveness, can be differentiated from human iPS cells.

We also confirmed the presence of adipocytes after transplantation of differentiated human iPS and ES cells. We

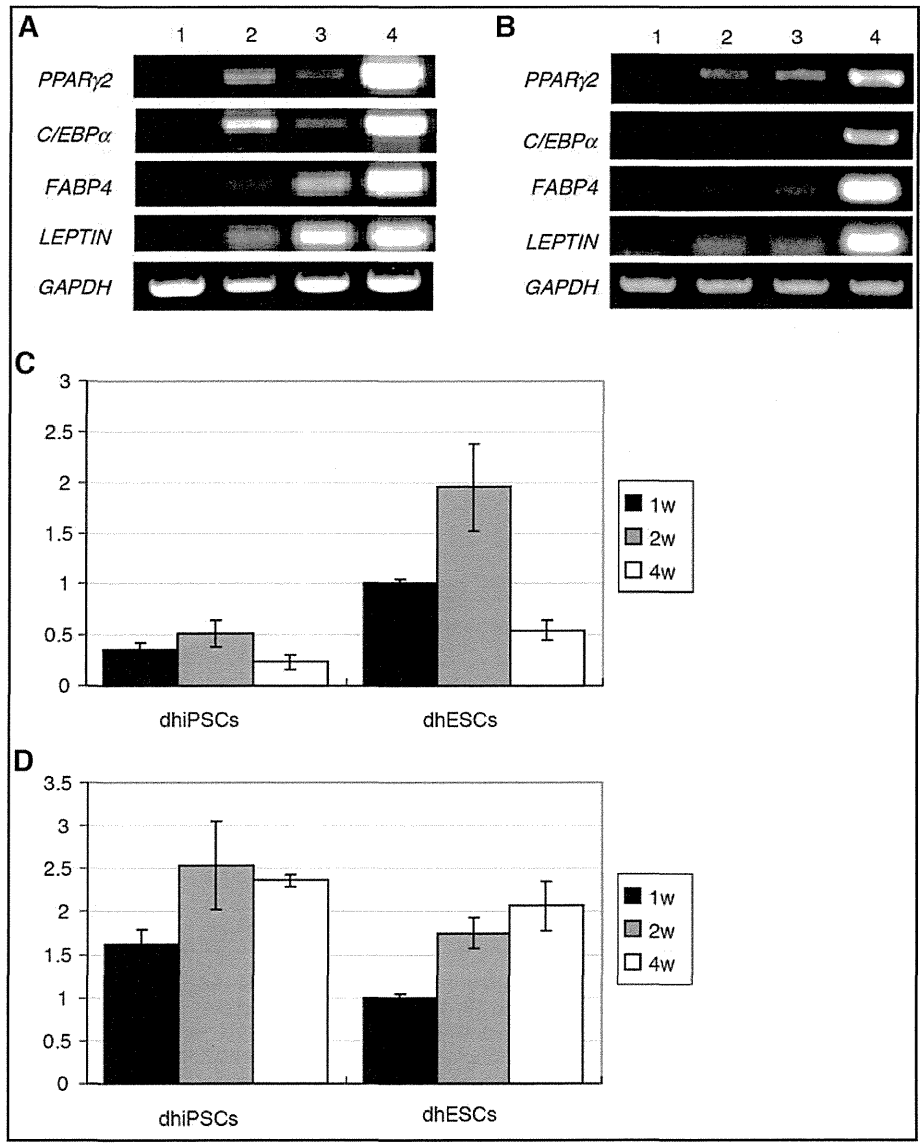

FIG. 5. Gene expression of adipocyte markers in transplanted cells. **(A, B)** Total RNA from transplanted cells (differentiated G4 and differentiated H9) was analyzed by RT-PCR at 2 **(A)** and 4 **(B)** weeks after transplantation. Lane 1: undifferentiated iPS cells (G4), lane 2: differentiated G4, lane 3: differentiated H9, lane 4: adipocytes derived from human bone marrow-derived mesenchymal stem cells. **(C, D)** Gene expression of human leptin **(C)** and PPARγ2 **(D)** was assessed by quantitative real-time PCR. Relative mRNA levels at 1, 2, and 4 weeks after transplantation of differentiated G4 (dhiPSCs) and differentiated H9 (dhESCs) were shown in *black*, *gray*, and *white bars*, respectively. Data represent ratios of the mRNA levels in samples of interest to the level in samples of differentiated H9 at 1 week after transplantation, respectively. Data are expressed as mean ± standard error from duplicate experiments ($n=5$). RT-PCR, reverse transcription polymerase chain reaction.

studied whether in vitro-differentiated adipocyte-derived human PS cells survived or not. When human iPS and ES cells are subjected to in vitro adipogenic induction via EB formation, the derivatives make up a heterogeneous population that includes adipocytes, preadipocytes, residual undifferentiated cells, and other cell types. Thus, adipocytes in transplanted Matrigel could be derived from any of these cell types after transplantation.

Time course analysis showed that the presence of adipocytes was confirmed at 1 week after transplantation of differentiated iPS and ES cells. Then, relative adipocyte areas peaked at 2 weeks. The adipocytes at 2 weeks after transplantation exhibited little or no proliferative capacity compared to immature neuroectodermal cells derived from undifferentiated iPS cells. Adipocytes were still present at 4 weeks. These findings indicate that adipocytes survive and maintain the differentiated state for 4 weeks after transplantation. Further, adipocytes described above were not seen in transplantation of undifferentiated iPS cells.

In that context, we hypothesize that the presence of adipocytes in transplanted Matrigel reflects the survival and maintenance of iPS and ES cells differentiated in vitro, although in vivo differentiation of preadipocytes may also contribute to the adipocytes seen in Matrigel after transplantation. Adipocytes as well as skeletal muscle cells, osteocytes, and chondrocytes are thought to be derived from mesenchymal progenitor cells [42,43]. Human mesenchymal stem cells have a characteristic surface antigen profile. Mesenchymal progenitor cells derived from human PS cells are enriched by sorting CD73- or CD105-positive cells [14,33,34,38]. We investigated the presence of mesenchymal progenitor cells in differentiated iPS and ES cells with adipogenic cocktail just before the transplantation. The expression of these surface antigens was analyzed in differentiated iPS and ES cells after the treatment with adipogenic cocktail. However, these representative surface antigens of human mesenchymal stem cells were not detected in differentiated iPS and ES cells (Supplementary Fig. S5), suggesting that

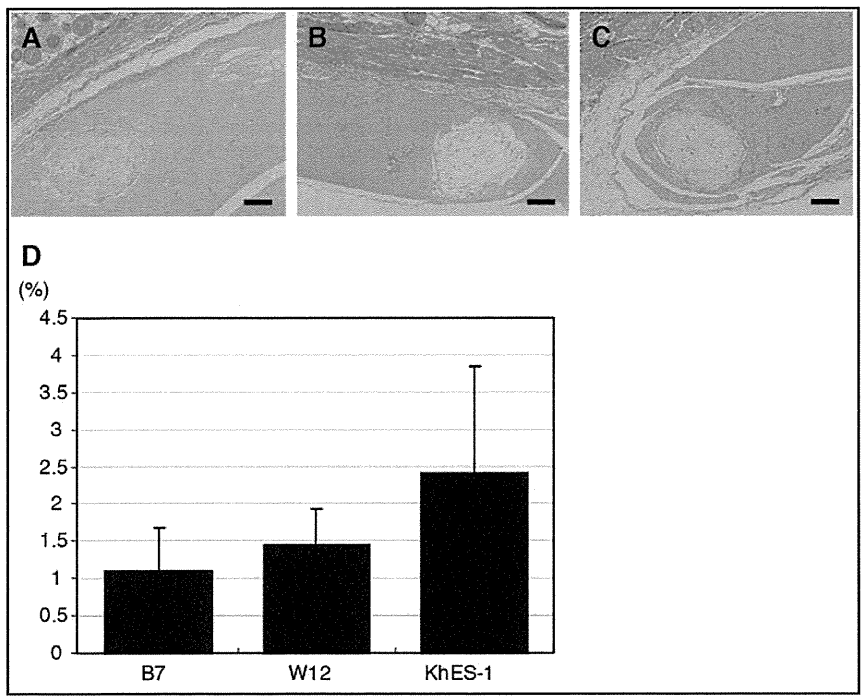

FIG. 6. Transplantation of adipocytes derived from other human pluripotent stem cells. **(A–C)** Transplanted cells were stained with HE. Morphological features of implanted Matrigel containing differentiated B7 **(A)**, W12 **(B)**, and KhES-1 **(C)** after 2 weeks. Scale bars = 100 μm. **(D)** Relative adipocyte areas at 2 weeks after transplantation of differentiated B7, W12, and KhES-1. Data are expressed as mean ± standard error. At least six sections from three samples were analyzed for each group.

mesenchymal progenitor cells are rare populations in differentiated iPS and ES cells after adipogenic induction at that point although mesenchymal progenitor cells may reside in derivatives from human PS cells at an earlier time point of this differentiation protocol.

Transplantation of mature adipocytes often results in graft loss caused by direct reduction of the number of viable adipocytes [22]. Transplantation of mature adipocytes together with adipose-derived stem cells significantly improves survival times and graft volumes, as compared with transplantation of mature adipocytes alone [21,44]. Thus, cotransplantation of mature adipocytes and preadipocytes derived from human iPS and ES cells may be advantageous for graft survival. Establishing a lineage-specific adipocyte differentiation protocol and the methods for the purification of adipocyte progenitors derived from human PS cells will be essential for the success of future cell therapies using adipocytes derived from human iPS cells.

Adipose tissue is now known to be a bona fide endocrine organ, which secretes a variety of adipocytokines, including leptin. Generalized lipodystrophy is caused by a profound deficiency in adipose tissue, which leads to diabetes with marked insulin resistance, hypertriglyceridemia, and ectopic lipid accumulation. We and others have established the efficacy and safety of long-term leptin replacement therapy for generalized lipodystrophy [45–50], but this therapy does not rescue these patients from their generalized lack of adipose tissue. The only complete cure for these patients would be replenishment of adipose tissue or adipocytes. Indeed, transplantation of adipose tissue or adipocyte progenitors has been demonstrated to ameliorate metabolic disorders in animal models of lipodystrophy [20,51]. Generalized lipodystrophy is classified into two types, congenital and acquired lipodystrophy. In the case of congenital lipodystrophy, we need to repair gene mutation of the patient-specific iPS cells for cell therapy. On the other hand, in the case of acquired lipodystrophy, iPS cells are expected to differentiate into adipocytes. However, successful engraftment of adipocytes derived from human iPS cells may be affected by host factors. Then, in consideration of allogeneic transplantation, iPS cell banking is now discussed, and some groups proposed clinical application of iPS cells from HLA homologous donors [52,53]. Transplantation using those allogeneic iPS cells can decrease or minimize the risk of immune rejection. Human iPS cell-derived adipocytes from patients or HLA homologous donors are a new strategy for the treatment of lipodystrophy.

In our transplantation studies, adipocytes derived from differentiated iPS (G4) and ES (H9) cells were clearly observed, whereas adipocytes derived from other human iPS cell lines (B7 and W12) or another human ES cell line (KhES-1) were observed less frequently. This suggests there is diversity among these cell lines with respect to the survival and maintenance of adipocytes. It was previously reported that there are marked differences in differentiation propensity among human ES cell lines [54]. One possible explanation is that these differences are attributable to the difference of in vitro adipogenic differentiation potential among these cell lines caused by their genetic backgrounds, sites of transgene integration, and epigenetic states. Further studies will be needed to clarify the mechanism underlying the observed differences.

In summary, the present study demonstrates that human iPS and ES cells can differentiate into adipocytes with functional properties and that adipocytes derived from human iPS and ES cells can survive and maintain the differentiated properties in vivo for at least 4 weeks after transplantation. Establishment of refined adipocyte differentiation protocol of human iPS and ES cells and the transplantation method of adipocytes derived from human iPS and ES cells will contribute to understanding the pathophysiology of metabolic

diseases such as obesity and lipodystrophy as well as to future therapeutic applications.

Acknowledgments

We thank S. Yamanaka and K. Takahashi (Center for iPS Cell Research and Application) for providing human iPS cells and technical assistance of generating human iPS cells. We thank N. Nakatsuji (Institute for Frontier Medical Science, Kyoto University) for providing human ES cells. We thank A. Ryu and M. Nagamoto for technical assistance. This work was supported in part by research grants from the Ministry of Education, Culture, Sports, Science and Technology of Japan, including Grant-in-Aid for Scientific Research on Innovative Areas (research in a proposed research area). "Molecular Basis and Disorders of Control of Appetite and Fat Accumulation" research project no. 22126001; the Ministry of Health, Labour and Welfare of Japan; the Takeda Medical Research Foundation; the Smoking Research Foundation; Suzuken Memorial Foundation; Japan Foundation of Applied Enzymology; Novo Nordisk Insulin Research Award; and Lilly Education and Research Grant office.

Author Disclosure Statement

The authors declare no potential conflict of interests.

References

1. Takahashi K, K Tanabe, M Ohnuki, M Narita, T Ichisaka, K Tomoda and S Yamanaka. (2007). Induction of pluripotent stem cells from adult human fibroblasts by defined factors. Cell 131:861–872.
2. Yu J, MA Vodyanik, K Smuga-Otto, J Antosiewicz-Bourget, JL Frane, S Tian, J Nie, GA Jonsdottir, V Ruotti, et al. (2007). Induced pluripotent stem cell lines derived from human somatic cells. Science 318:1917–1920.
3. Park IH, R Zhao, JA West, A Yabuuchi, H Huo, TA Ince, PH Lerou, MW Lensch and GQ Daley. (2008). Reprogramming of human somatic cells to pluripotency with defined factors. Nature 451:141–146.
4. Chambers SM, CA Fasano, EP Papapetrou, M Tomishima, M Sadelain and L Studer. (2009). Highly efficient neural conversion of human ES and iPS cells by dual inhibition of SMAD signaling. Nat Biotechnol 27:275–280.
5. Dimos JT, KT Rodolfa, KK Niakan, LM Weisenthal, H Mitsumoto, W Chung, GF Croft, G Saphier, R Leibel, et al. (2008). Induced pluripotent stem cells generated from patients with ALS can be differentiated into motor neurons. Science 321:1218–1221.
6. Soldner F, D Hockemeyer, C Beard, Q Gao, GW Bell, EG Cook, G Hargus, A Blak, O Cooper, et al. (2009). Parkinson's disease patient-derived induced pluripotent stem cells free of viral reprogramming factors. Cell 136:964–977.
7. Osakada F, ZB Jin, Y Hirami, H Ikeda, T Danjyo, K Watanabe, Y Sasai and M Takahashi. (2009). *In vitro* differentiation of retinal cells from human pluripotent stem cells by small-molecule induction. J Cell Sci 122:3169–3179.
8. Choi KD, J Yu, K Smuga-Otto, G Salvagiotto, W Rehrauer, M Vodyanik, J Thomson and I Slukvin. (2009). Hematopoietic and endothelial differentiation of human induced pluripotent stem cells. Stem Cells 27:559–567.
9. Zhang J, GF Wilson, AG Soerens, CH Koonce, J Yu, SP Palecek, JA Thomson and TJ Kamp. (2009). Functional cardiomyocytes derived from human induced pluripotent stem cells. Circ Res 104:e30–e41.
10. Sullivan GJ, DC Hay, IH Park, J Fletcher, Z Hannoun, CM Payne, D Dalgetty, JR Black, JA Ross, et al. (2010). Generation of functional human hepatic endoderm from human induced pluripotent stem cells. Hepatology 51:329–335.
11. Hockemeyer D, F Soldner, EG Cook, Q Gao, M Mitalipova and R Jaenisch. (2008). A drug-inducible system for direct reprogramming of human somatic cells to pluripotency. Cell Stem Cell 3:346–353.
12. Maherali N, T Ahfeldt, A Rigamonti, J Utikal, C Cowan and K Hochedlinger. (2008). A high-efficiency system for the generation and study of human induced pluripotent stem cells. Cell Stem Cell 3:340–345.
13. Taura D, M Noguchi, M Sone, K Hosoda, E Mori, Y Okada, K Takahashi, K Homma, N Oyamada, et al. (2009). Adipogenic differentiation of human induced pluripotent stem cells: comparison with that of human embryonic stem cells. FEBS Lett 583:1029–1033.
14. Lian Q, Y Zhang, J Zhang, HK Zhang, X Wu, Y Zhang, FF Lam, S Kang, JC Xia, et al. (2010). Functional mesenchymal stem cells derived from human induced pluripotent stem cells attenuate limb ischemia in mice. Circulation 121:1113–1123.
15. Rhee YH, JY Ko, MY Chang, SH Yi, D Kim, CH Kim, JW Shim, AY Jo, BW Kim, et al. (2011). Protein-based human iPS cells efficiently generate functional dopamine neurons and can treat a rat model of Parkinson disease. J Clin Invest 121:2326–2335.
16. Liu H, Y Kim, S Sharkis, L Marchionni and YY Jang. (2011). *In vivo* liver regeneration potential of human induced pluripotent stem cells from diverse origins. Sci Transl Med 3:82ra39.
17. Nori S, Y Okada, A Yasuda, O Tsuji, Y Takahashi, Y Kobayashi, K Fujiyoshi, M Koike, Y Uchiyama, et al. (2011). Grafted human-induced pluripotent stem-cell-derived neurospheres promote motor functional recovery after spinal cord injury in mice. Proc Natl Acad Sci U S A 108:16825–16830.
18. Garg A. (2011). Clinical review#: Lipodystrophies: genetic and acquired body fat disorders. J Clin Endocrinol Metab 96:3313–3325.
19. Semple RK, DB Savage, EK Cochran, P Gorden and S O'Rahilly. (2011). Genetic syndromes of severe insulin resistance. Endocr Rev 32:498–514.
20. Gavrilova O, B Marcus-Samuels, D Graham, JK Kim, GI Shulman, AL Castle, C Vinson, M Eckhaus and ML Reitman. (2000). Surgical implantation of adipose tissue reverses diabetes in lipoatrophic mice. J Clin Invest 105:271–278.
21. ELFadl D, V Garimella, TK Mahapatra, PL McManus and PJ Drew. (2010). Lipomodelling of the breast: a review. Breast 19:202–209.
22. Chan CW, SJ McCulley and RD Macmillan. (2008). Autologous fat transfer—a review of the literature with a focus on breast cancer surgery. J Plast Reconstr Aesthet Surg 61:1438–1448.
23. Zeve D, W Tang and J Graff. (2009). Fighting fat with fat: the expanding field of adipose stem cells. Cell Stem Cell 5:472–481.
24. Locke M, V Feisst and PR Dunbar. (2011). Concise review: human adipose-derived stem cells: separating promise from clinical need. Stem Cells 29:404–411.
25. Alhadlaq A, M Tang and JJ Mao. (2005). Engineered adipose tissue from human mesenchymal stem cells maintains predefined shape and dimension: implications in soft tissue augmentation and reconstruction. Tissue Eng 11:556–566.
26. Choi YS, SN Park and H Suh. (2005). Adipose tissue engineering using mesenchymal stem cells attached to injectable PLGA spheres. Biomaterials 26:5855–5863.

27. Hong L, IA Peptan, A Colpan and JL Daw. (2006). Adipose tissue engineering by human adipose-derived stromal cells. Cells Tissues Organs 183:133–140.
28. Hillel AT, S Varghese, J Petsche, MJ Shamblott and JH Elisseeff. (2009). Embryonic germ cells are capable of adipogenic differentiation *in vitro* and *in vivo*. Tissue Eng Part A 15:479–486.
29. Thomson JA, J Itskovitz-Eldor, SS Shapiro, MA Waknitz, JJ Swiergiel, VS Marshall and JM Jones. (1998). Embryonic stem cell lines derived from human blastocysts. Science 282:1145–1147.
30. Suemori H, K Yasuchika, K Hasegawa, T Fujioka, N Tsuneyoshi and N Nakatsuji. (2006). Efficient establishment of human embryonic stem cell lines and long-term maintenance with stable karyotype by enzymatic bulk passage. Biochem Biophys Res Commun 345:926–932.
31. Noguchi M, K Hosoda, J Fujikura, M Fujimoto, H Iwakura, T Tomita, T Ishii, N Arai, M Hirata, et al. (2007). Genetic and pharmacological inhibition of Rho-associated kinase II enhances adipogenesis. J Biol Chem 282:29574–29583.
32. Tsuji W, T Inamoto, H Yamashiro, T Ueno, H Kato, Y Kimura, Y Tabata and M Toi. (2009). Adipogenesis induced by human adipose tissue-derived stem cells. Tissue Eng Part A 15:83–93.
33. Ahfeldt T, RT Schinzel, YK Lee, D Hendrickson, A Kaplan, DH Lum, R Camahort, F Xia, J Shay, et al. (2012). Programming human pluripotent stem cells into white and brown adipocytes. Nat Cell Biol 14:209–219.
34. Barberi T, LM Willis, ND Socci and L Studer. (2005). Derivation of multipotent mesenchymal precursors from human embryonic stem cells. PLoS Med 2:e161.
35. Xiong C, CQ Xie, L Zhang, J Zhang, K Xu, M Fu, WE Thompson, LJ Yang and YE Chen. (2005). Derivation of adipocytes from human embryonic stem cells. Stem Cells Dev 14:671–675.
36. Olivier EN, AC Rybicki and EE Bouhassira. (2006). Differentiation of human embryonic stem cells into bipotent mesenchymal stem cells. Stem Cells 24:1914–1922.
37. van Harmelen V, G Astrom, A Stromberg, E Sjolin, A Dicker, O Hovatta and M Ryden. (2007). Differential lipolytic regulation in human embryonic stem cell-derived adipocytes. Obesity (Silver Spring) 15:846–852.
38. Lian Q, E Lye, K Suan Yeo, E Khia Way Tan, M Salto-Tellez, TM Liu, N Palanisamy, RM El Oakley, EH Lee, B Lim and SK Lim. (2007). Derivation of clinically compliant MSCs from CD105+, CD24- differentiated human ESCs. Stem Cells 25:425–436.
39. Lee G, H Kim, Y Elkabetz, G Al Shamy, G Panagiotakos, T Barberi, V Tabar and L Studer. (2007). Isolation and directed differentiation of neural crest stem cells derived from human embryonic stem cells. Nat Biotechnol 25:1468–1475.
40. Mahmood A, L Harkness, HD Schroder, BM Abdallah and M Kassem. (2010). Enhanced differentiation of human embryonic stem cells to mesenchymal progenitors by inhibition of TGF-beta/activin/nodal signaling using SB-431542. J Bone Miner Res 25:1216–1233.
41. Ahmadian M, RE Duncan and HS Sul. (2009). The skinny on fat: lipolysis and fatty acid utilization in adipocytes. Trends Endocrinol Metab 20:424–428.
42. Gesta S, YH Tseng and CR Kahn. (2007). Developmental origin of fat: tracking obesity to its source. Cell 131:242–256.
43. Billon N, MC Monteiro and C Dani. (2008). Developmental origin of adipocytes: new insights into a pending question. Biol Cell 100:563–575.
44. Tremolada C, G Palmieri and C Ricordi. (2010). Adipocyte transplantation and stem cells: plastic surgery meets regenerative medicine. Cell Transplant 19:1217–1223.
45. Shimomura I, RE Hammer, S Ikemoto, MS Brown and JL Goldstein. (1999). Leptin reverses insulin resistance and diabetes mellitus in mice with congenital lipodystrophy. Nature 401:73–76.
46. Ebihara K, Y Ogawa, H Masuzaki, M Shintani, F Miyanaga, M Aizawa-Abe, T Hayashi, K Hosoda, G Inoue, et al. (2001). Transgenic overexpression of leptin rescues insulin resistance and diabetes in a mouse model of lipoatrophic diabetes. Diabetes 50:1440–1448.
47. Oral EA, V Simha, E Ruiz, A Andewelt, A Premkumar, P Snell, AJ Wagner, AM DePaoli, ML Reitman, et al. (2002). Leptin-replacement therapy for lipodystrophy. N Engl J Med 346:570–578.
48. Ebihara K, H Masuzaki and K Nakao. (2004). Long-term leptin-replacement therapy for lipoatrophic diabetes. N Engl J Med 351:615–616.
49. Ebihara K, T Kusakabe, M Hirata, H Masuzaki, F Miyanaga, N Kobayashi, T Tanaka, H Chusho, T Miyazawa, et al. (2007). Efficacy and safety of leptin-replacement therapy and possible mechanisms of leptin actions in patients with generalized lipodystrophy. J Clin Endocrinol Metab 92:532–541.
50. Nakao K, A Yasoda, K Ebihara, K Hosoda and M Mukoyama. (2009). Translational research of novel hormones: lessons from animal models and rare human diseases for common human diseases. J Mol Med 87:1029–1039.
51. Rodeheffer MS, K Birsoy and JM Friedman. (2008). Identification of white adipocyte progenitor cells *in vivo*. Cell 135:240–249.
52. Okita K, Y Matsumura, Y Sato, A Okada, A Morizane, S Okamoto, H Hong, M Nakagawa, K Tanabe, et al. (2011). A more efficient method to generate integration-free human iPS cells. Nat Methods 8:409–412.
53. Taylor CJ, S Peacock, AN Chaudhry, JA Bradley and EM Bolton. (2012). Generating an iPSC bank for HLA-matched tissue transplantation based on known donor and recipient HLA types. Cell Stem Cell 11:147–152.
54. Osafune K, L Caron, M Borowiak, RJ Martinez, CS Fitz-Gerald, Y Sato, CA Cowan, KR Chien and DA Melton. (2008). Marked differences in differentiation propensity among human embryonic stem cell lines. Nat Biotechnol 26:313–315.

Address correspondence to:
Dr. Kiminori Hosoda
Department of Medicine and Clinical Science
Kyoto University Graduate School of Medicine
54 Shogoin Kawahara-cho, Sakyo-ku
Kyoto 606-8507
Japan

E-mail: kh@kuhp.kyoto-u.ac.jp

Dr. Kazuwa Nakao
Department of Medicine and Clinical Science
Kyoto University Graduate School of Medicine
54 Shogoin Kawahara-cho, Sakyo-ku
Kyoto 606-8507
Japan

E-mail: nakao@kuhp.kyoto-u.ac.jp

Received for publication February 27, 2013
Accepted after revision June 10, 2013
Prepublished on Liebert Instant Online June 10, 2013

Original Article
CLINICAL TRIALS: BEHAVIOR, PHARMACOTHERAPY, DEVICES, SURGERY

Obesity

Early Changes of Abdominal Adiposity Detected with Weekly Dual Bioelectrical Impedance Analysis during Calorie Restriction

Midori Ida[1], Masakazu Hirata[1], Shinji Odori[1], Eisaku Mori[1], Eri Kondo[1], Junji Fujikura[1], Toru Kusakabe[1], Ken Ebihara[1], Kiminori Hosoda[1,2] and Kazuwa Nakao[1]

Objective: To elucidate early change of intra-abdominal fat in response to calorie restriction in patients with obesity by weekly evaluation using a dual bioelectrical impedance analysis (Dual BIA) instrument.
Design and Methods: For 67 Japanese patients with obesity, diabetes, or metabolic syndrome, intra-abdominal fat area (IAFA), initially with both Dual BIA and computed tomography (CT), and in subsequent weeks of calorie restriction, with Dual BIA were measured.
Results: IAFA by Dual BIA (Dual BIA-IAFA) correlated well with IAFA by CT (CT-IAFA) in obese patients ($r = 0.821$, $P < .0001$, $n = 67$). Ten males and 9 females (age 49.0 ± 14.4 years, BMI 33.2 ± 7.3 kg/m^2) lost more than 5% of baseline body weight (BW) in 3 weeks, and their Dual BIA-IAFA, BW, and WC decreased by 18.9%, 5.3%, and 3.8%, respectively ($P < .05$, ANCOVA).
Conclusion: Dual BIA instrument could detect the weekly change of Dual BIA-IAFA under calorie restriction in obese patients and demonstrated a substantially larger change of IAFA compared with changes of BW and WC in early weeks. This observation corroborates the significance of evaluating IAFA as a biomarker for obesity, and indicates the clinical usefulness of the Dual BIA instrument.

Obesity (2013) **21**, E350-E353. doi:10.1002/oby.20300

Introduction

Abdominal adiposity is associated with development of obesity and metabolic abnormalities in obesity-related diseases (1-3). The adipose tissue distribution has been quantitatively evaluated by computed tomography (CT) (4) or magnetic resonance imaging (MRI) (5), and intra-abdominal fat area (IAFA) is used as a clinical parameter of abdominal adiposity (6). Although waist circumference (WC) is casually employed to evaluate abdominal adiposity (7), WC is known to reflect both the intra-abdominal and the subcutaneous abdominal adiposity. In addition, the correlation of WC with intra-abdominal adiposity is influenced by age and sex as shown in epidemiological studies (5). Thus, WC does not necessarily provide the precise information about abdominal fat distribution. Therefore, a new practical method for detecting early change in abdominal adiposity is needed to elucidate its consequence during acute phase of calorie restriction in obesity treatment (8). There have been a few proposals of methods (9,10) that assess IAFA as alternatives to CT (4) or MRI (5). However, there has been no report on clinical application of these methods analyzing the weekly change of IAFA during calorie restriction. We have developed the dual bioelectrical impedance analysis (Dual BIA) instrument that can determine IAFA by measuring truncal impedance and surface impedance at the abdomen separately, each of which reflects the truncal adiposity and the subcutaneous adiposity respectively (11-13). The Dual BIA instrument has been optimized with aims at robustness for use in a wide range of human variation by analyzing the size of effect that each parameter, such as age and gender, can have on the calculation outcomes utilizing information technology (11-13). In this study, we report on application of the Dual BIA instrument to compare the weekly change in IAFA and body weight (BW) of obese patients with the metabolic syndrome or diabetes mellitus resulting from calorie restriction.

Methods

Dual BIA method and instrumentation

Dual BIA instrument calculates the cross-sectional area of intra-abdominal fat at the level of umbilicus based on the measurement of electrical potentials resulting from applying small electrical currents in two different body space. Principles of IAFA determination by Dual BIA instrument have been described previously (11-13) in detail. Briefly, the Dual BIA instrument consists of bioelectrical impedance

[1] Department of Medicine and Clinical Science, Kyoto University Graduate School of Medicine, Sakyo-ku, Kyoto, Japan. Correspondence: Masakazu Hirata (mhirata@kuhp.kyoto-u.ac.jp) [2] Department of Human Health Science, Kyoto University Graduate School of Medicine, Sakyo-ku, Kyoto, 606-8507, Japan

Disclosure: The authors declared no conflict of interest.
Funding agencies: This work was supported in part by research grants from the Ministry of Education, Culture, Sports, Science and Technology of Japan including Grant in Aid for Scientific Research on Innovative Areas (Research in a proposed research area) "Molecular Basis and Disorders of Control of Appetite and Fat Accumulation", the Ministry of Health, Labour and Welfare of Japan, the Takeda Medical Research Foundation, the Smoking Research Foundation, Suzuken Memorial Foundation, Japan Foundation of Applied Enzymology, Novo Nordisk Insulin Research Award, Lilly Education and Research Grant Office.
Received: 8 May 2012 **Accepted:** 25 November 2012 **Published online 2 January 2013. doi:10.1002/oby.20300**

component that measures truncal and surface impedance of the body, and a device that measures physical size of the abdomen. The two sets of electrodes are for limb and truncal placement. The limb electrodes consist of four clip-on electrodes placed on wrists and ankles. The truncal electrodes are eight pairs of electrodes 6 cm apart longitudinally that are fixed to a belt where four pairs each for front and back are positioned at an equal inter-electrode distance. The belt is adjustable so that the electrodes are positioned centered on mid-sagittal line at the level of umbilicus in supine position. The truncal impedance is measured by applying electrical currents between upper and lower limb leads and reading voltage from the electrodes around the abdominal circumference. The surface impedance is measured by applying and reading voltage from the abdominal circumferential electrodes. IAFA by Dual BIA (Dual BIA-IAFA) is calculated as follows.

$$\text{Dual BIA} - \text{IAFA} = \alpha_1 A + \alpha_2 B^2 - \alpha_3 \left(A^2 + B^2\right)^{1/2} Z_s - \alpha_4 / Z_t + \varepsilon \quad (1)$$

A: abdominal antero-posterior diameter, B: abdominal transverse diameter, Z_s: surface impedance, Z_t: truncal impedance, ε: residual constant.

There was a good agreement of Dual BIA-IAFA and IAFA measured by CT (CT-IAFA) with the correlation coefficient of 0.888 ($n = 98$, $P < .001$) (13).

Patient selection

The study was performed according to the protocol approved by Kyoto University Medical Ethics Review Board (no. 080116). The patient gave a written consent to participate in this study which took place at the endocrinology and metabolism ward of Kyoto University Hospital. We collected data from 67 Japanese patients (36 males and 31 females; mean ± SD age, 54.7 ± 14.7 years, BMI 29.3 ± 6.5 kg/m^2) with obesity ($n = 56$), diabetes mellitus ($n = 45$), or the metabolic syndrome ($n = 38$) who were hospitalized for calorie restriction therapy or diet education, and had measurement of IAFA by both Dual BIA method and CT method at the start of calorie restriction. Obesity was diagnosed as BMI 25.0, and metabolic syndrome was diagnosed according to 2005 Japanese criteria of metabolic syndrome (14). Average daily calorie intake was 1437.3 ± 201.4 kcal/day (19.3 ± 4.3 kcal/ideal BW). Out of 67 patients, 35 patients could be followed for longer than 3 weeks, while the other patients were discharged earlier after examination of complications and diet and lifestyle education. Total daily energy was varied individually during hospitalization based on consultation between the patient, a dietician, and a physician. Out of 35 patients who had their Dual BIA-IAFA monitored every week for at least 3 weeks (four times), 19 patients lost more than 5% of baseline BW, and were included in the analysis of weekly change in Dual BIA-IAFA, WC, and BW during weight reduction.

Measurement of Dual BIA, CT, and anthropometric parameters

Dual BIA-IAFA was measured every week in the morning before breakfast depending on individual patient's treatment schedule (Figure 1A). Abdominal CT was performed for calculation of CT-IAFA within 7 days before the initial Dual BIA-IAFA measurement. CT-IAFA was calculated at umbilical level by the software, Virtual Place Lexus (AZE of Japan, Ltd). BW was measured to the nearest 0.1 kg in the morning of the Dual BIA-IAFA measurement.

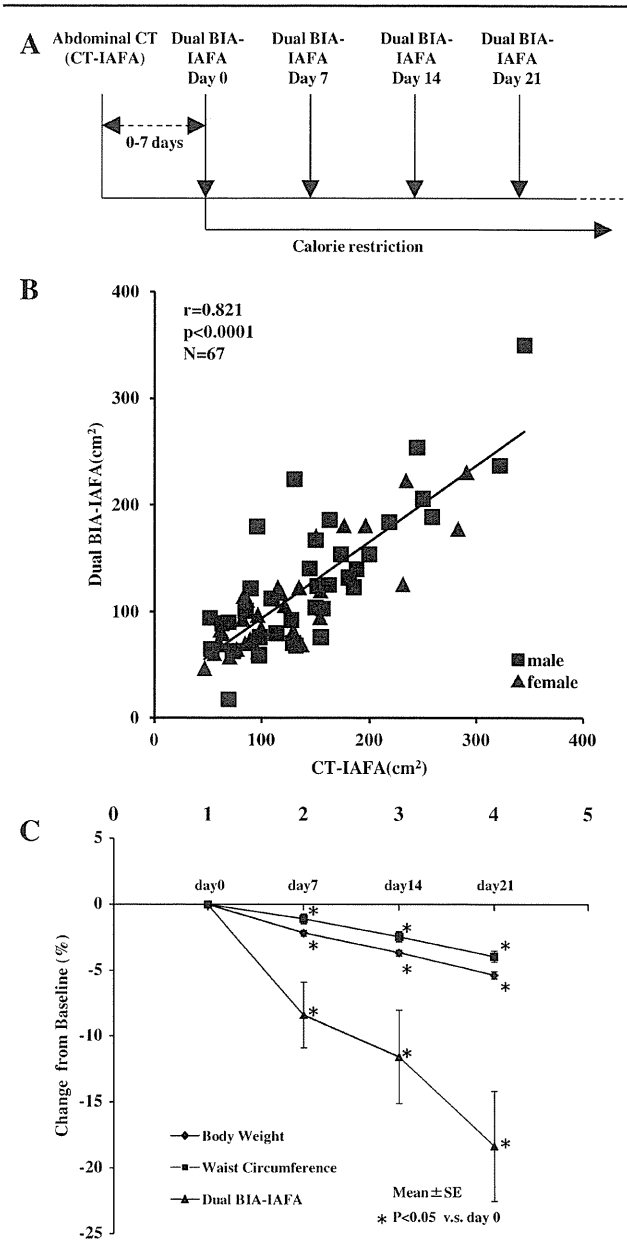

FIGURE 1 A: Diagram of IAFA assessment schedule during the calorie restriction. Patients started fixed calorie diet within 7 days of taking the abdominal CT image. Dual BIA-IAFA assessment took place in the morning before meal every week. CT imaging took place either in the morning or in the afternoon. **B**: Correlation between CT-IAFA and BIA-IAFA in 67 patients who were with obesity-related disorders. Square symbols: male, Triangle symbols: female. $r = 0.821$, $P < .001$ by Pearson's analysis. **C**: Weekly change of Dual BIA-IAFA plotted along with BW and WC during weight loss. Nineteen patients who underwent the calorie restriction and had abdominal CT examined at baseline were monitored for their anthropometric parameters and Dual BIA-IAFA weekly for at least 3 weeks. They lost more than 5% of BW during the period. Size of the change from baseline values (mean ± SE) is expressed as %. *$P < .05$ by Student's paired t-test.

WC was measured at the level of the umbilicus to the nearest 0.1 cm in the standing position at the end of expiration while breathing gently at the time of Dual BIA measurement.

Statistical methods

Correlation between values obtained by Dual BIA and CT were evaluated using Pearson's correlation analysis. Weekly values of Dual BIA-IAFA, BW, and WC were compared with the baseline values of day 0 by Student's paired *t*-test. Analysis of covariance was applied for comparison of Dual BIA-IAFA, BW, and WC at week 3.

Results

In 67 patients with obesity and related conditions, Dual BIA-IAFA correlated well with CT-IAFA ($r = 0.821$, $P < .0001$) (Figure 1B).

Thirty-five (17 males and 18 females) out of 67 patients were monitored with Dual BIA for longer than 3 weeks, and 19 (10 males and 9 females) out of 35 patients achieved weight loss of more than 5% of the initial BW. In order to elucidate the change in IAFA during weight loss, Dual BIA-IAFA, BW, and WC of the 19 patients were analyzed. Baseline characteristics of the 19 patients were (mean ± SD); age, 49.0 ± 14.4 years, height 163.0 ± 10.5 cm, BMI 33.2 ± 7.3 kg/m^2, and CT-IAFA 143.6 ± 47.4 cm^2. BW, WC, and Dual BIA-IAFA at baseline and at week 3 were: 89.2 ± 26.2 kg and 84.5 ± 25.1 kg, 110.6 ± 14.1 cm and 106.0 ± 14.2 cm, and 150.4 ± 73.7 cm^2 and 124.3 ± 70.3 cm^2, respectively.

Figure 1C shows the weekly change of Dual BIA-IAFA, BW, and WC in 19 patients whose BW decreased more than 5% during the 3 weeks of monitoring. Dual BIA-IAFA, BW and WC showed a significant reduction after 1 week during the calorie restriction compared with the baseline values ($P < .05$). Dual BIA-IAFA decreased every week for the initial 3 weeks and the average reduction in Dual BIA-IAFA was 18.9%, which was larger than in BW (5.3%) and WC (3.8%) (ANCOVA, $P < .05$).

Discussion

The present study demonstrates that the weekly change in IAFA can be detected with the Dual BIA instrument during the calorie restriction. Due to the practical limitations such as instrumentation and cost, CT and MRI are unsuitable for weekly monitoring of change in IAFA. There is also a problem of X-ray exposure in CT scanning. Consequently, it has been impractical to monitor IAFA weekly or frequently, in clinical follow-up period with CT or MRI. There have been several attempts to evaluate the IAFA by BIA (9-13). They include calculation from whole body impedance and from measuring abdominal impedance by the electrodes placed on the abdomen (9,10). Some of the estimates of IAFA incorporate gender and age of the subject in order to attain high correlation with CT (9,10). In contrast, Dual BIA, which is a method that is not dependent on external variables, such as gender or age, had shown a good correlation between Dual BIA-IAFA and CT-IAFA (11-13). In the present study, we confirmed the good correlation of Dual BIA-IAFA and CT-IAFA in obese patients. The correlation coefficient for the Dual BIA-IAFA and CT-IAFA was 0.821 ($n = 67$) with our subjects whose average BMI was 29.3. This indicates that Dual BIA produced reliable measurements with obesity patients and the result was comparable to the correlation coefficient of 0.888 obtained with subjects whose average BMI was around 25 (13). It must be noted that CT-IAFA and Dual BIA-IAFA was not measured on the same day in the present study, unlike the previous report in which Dual BIA- and CT-IAFA was taken on the same day (13), and therefore direct comparison has its limitations. By applying Dual BIA to monitoring the weekly change of individual body component during the calorie restriction, we could detect the characteristic change of IAFA. The significant decrease in Dual BIA-IAFA, BW, and WC at week 1 supports the suitability of selecting 5% of BW change at week 3 as a criterion for including in weekly analysis of these parameters.

On average, IAFA showed a larger reduction than BW and WC during the initial 3 weeks of calorie restriction. The rapid response of intra-abdominal adipose tissue to calorie restriction has been suggested in an ultrasonography study that examined a portion of peritoneal fat thickness (15). The larger decrease of Dual BIA-IAFA observed is also in agreement with a study which showed larger reduction in IAFA evaluated with MRI than that of BW up to 12 weeks on very low calorie diet (16). Together with these results, the present study established that the intra-abdominal fat decreases rapidly in the initial period of calorie restriction by measuring Dual BIA-IAFA, and demonstrates the usefulness of monitoring the change in IAFA during the treatment of obesity and its related disorders.

Weakness of our study is that its design was not of a prospective weight reduction where every participant was prescribed daily calorie that could produce predetermined level of weight loss within the study period. Instead we selected participants that had their weight decreased by at least 5% in order to illustrate the change in abdominal adiposity on weekly basis. It is also of note that the BW and Dual BIA-IAFA at week 1 may be affected by salt restriction and loss of body water that is observed early in calorie restriction. Because of the small sample size, the observed change in Dual BIA-IAFA could be larger than actual change. It also depends on the precision of the instrument. In a separate population, the coefficient of variation was 7.6% (Ida, M. manuscript in preparation).

In conclusion, the present study demonstrated that Dual BIA instrument can be used to measure IAFA in obese patients, allows frequent measurement, and is useful for detecting the early change in IAFA during calorie restriction. Information thus obtained along with other changes in metabolic parameters will be indispensable for understanding the role of abdominal adiposity, and especially useful as a diagnostic marker for monitoring obesity and its related disorders (1). In addition, the instrument's safety and convenience could be suitable for large population studies.O

Acknowledgments

Authors thank all the volunteers who took part in the study, and Research and Development Department of Omron Healthcare Corporation for use of the Dual BIA instrument.

References

1. Matsuzawa Y. The role of fat topology in the risk of disease. *Int J Obes* 2008;32: S83-S92.